Freskida Goni, BSc

High-yield production and characterization of boron nitride nanosheets

MASTER'S THESIS

to achieve the university degree of

Master of Science

Master's degree programme: Chemistry

submitted to

Graz University of Technology

Supervisor

Univ.-Prof. Dipl.-Chem. Dr.rer.nat., Frank Uhlig

Institute for Inorganic Chemistry

Second supervisor

Mag.rer.nat. Dr.rer.nat., Angela Chemelli

Graz, July 2017

AFFIDAVIT

I declare that I have authored this thesis independently, that I have not used other than the declared sources/resources, and that I have explicitly indicated all material which has been quoted either literally or by content from the sources used. The text document uploaded to TUGRAZonline is identical to the present master‘s thesis.

Date

Signature

ACKNOWLEDGMENTS

First, I would like to thank Professor Frank Uhlig for believing in me and giving me the opportunity to work on this project. I am very grateful for all his supervision, support and help.

A big thank you to my supervisor and mentor Angela Chemelli, who has always been there for me, for guiding me and teaching me everything I needed to know. I appreciate her patience, motivation and support very much.

To the Polymer Competence Center Leoben, thank you for the financial support.

To Karin Wewerka, thank you for the TEM pictures.

I am very grateful for all my colleagues and friends whom I had the pleasure to meet at the Inorganic Institute of Graz University of Technology.

A special thank you goes to my parents, for always supporting me and believing in me more than I ever believed in myself.

Thank you to my family and friends.

Last but not least, a profound acknowledgment goes to my boyfriend, for being there for me through the years, through beautiful and hard times, for his love and encouragement.

There are no words to describe how grateful I am for all the opportunities I've had and especially, most of all for the people in my life. I wouldn't be where I am now, without you.

THANK YOU!

The only way of discovering the limits of the possible is to venture a little way past them into the impossible!

~ Arthur C. Clarke

ABSTRACT

Boron nitride nanosheets (BNNSs) have gained great attention as an interesting filler medium in the production of electrically insulating and thermally conductive polymer-based composite materials. Their wide band gap and high thermal conductivity make BNNSs a superior candidate for this application. However, one of the greatest barricades to the further investigation and production of these polymers is the lack of cost-effective methods for fabricating high yields of BNNSs.

This thesis work focuses on improving the liquid phase exfoliation method for the high-yield production of BNNSs, using sonication for the exfoliation of the nanosheets from the *h*-BN bulk crystal and centrifugation to separate the exfoliated nanosheets from the non-exfoliated ones. Different solvents were investigated as well as both, bath- and probe-type sonication method. Furthermore, a route for the exchange of the solvent from the one in which the liquid phase exfoliation was performed to a new one, more suitable for the incorporation and integration of the nanosheets as a filler material into a polymer matrix is demonstrated. The yields achieved reach up to approximately 23 % and a method on how to prepare around 1 g of BNNSs in just a few days is presented in this work.

Ultraviolet-visible spectroscopy (UV-Vis), dynamic light scattering (DLS), small angle X-ray scattering (SAXS) and transmission electron microscopy (TEM) were used for the characterization of the BNNSs.

Overall, this work presents an improved, cost-effective and fast method for the preparation of boron nitride nanosheets.

KURZFASSUNG

Bornitrid-Nanoplättchen (BNNSs) haben große Aufmerksamkeit als interessantes Füllstoff in der Produktion von elektrisch isolierenden und wärmeleitfähigen Verbundwerkstoffen auf Polymerbasis erregt. Ihre breite Bandabstand und hohe Wärmeleitfähigkeit machen BNNSs zu einem hervorragenden Kandidaten für diese Anwendung. Eine der größten Barrikaden für die weitere Untersuchung und Herstellung dieser Polymere ist jedoch der Mangel an kostengünstigen Methoden zur Herstellung hoher BNNSs-Ausbeuten.

Der Fokus dieser Arbeit war die Optimierung der Flüssigphasen-Exfolierungs-Methode für die Produktion von BNNSs in hohen Ausbeuten, unter Verwendung von Ultraschall für die Exfolierung hexagonalen Bornitrids und der Zentrifugation, um die exfolierten Nanoschichten von den nicht-exfolierten zu trennen. Es wurden verschiedene Lösungsmittel untersucht sowie sowohl die Bad- als auch die Sonden-Ultraschallmethode. Des Weiteren wird ein Weg für den Austausch des Lösungsmittels von dem, in dem die Flüssigphasen-Exfolierung durchgeführt wurde, zu einem neuen, das für den Einbau und die Integration der Nanoschichten als Füllstoffmaterial in eine Polymermatrix besser geeignet ist, demonstriert. Ausbeuten bis zu 23 % wurden erreicht. Es wird gezeigt, dass 1g BNNSs in nur wenig Tagen hergestellt werden kann.

BNNSs wurden mittels UV/Vis-Spektroskopie, dynamische Lichtstreuung (DLS), Kleinwinkel-Röntgenstreuung (SAXS) und Transmissions-Elektronen-Mikroskopie (TEM) charakterisiert.

Insgesamt präsentiert diese Arbeit eine verbesserte, kostengünstige und schnelle Methode zur Herstellung von Bornitrid-Nanoschichten.

CONTENTS

LIST OF ABBREVIATIONS

C:	Carbon atom
B:	Boron atom
N:	Nitrogen atom
BN:	Boron nitride
h-BN:	Hexagonal boron nitride
BNNS / BNNSs:	Boron nitride nanosheet / boron nitride nanosheets
0D:	Zero-dimensional
1D:	One-dimensional
2D:	Two- dimensional
3D:	Tree- dimensional
UV-Vis:	Ultraviolet-visible spectroscopy
DLS:	Dynamic light scattering
PCS:	Photo correlation spectroscopy
QELS:	Quasi-elastic light scattering
SAXS:	Small angle x-ray scattering
TEM:	Transmission electron microscopy
ACN:	Acetonitrile
IPA:	Isopropanol

NMP:	N-methyl-2-pyrrolidone
PEG_{200}:	$Polyethylenglycol_{200}$
DMF:	Dimethylformamide
TMDs:	Transition metal dichalcogenides
LDHs:	Layered double hydroxides
BP:	Black phosphorus
MOFs:	Metal organic frameworks
LPE:	Liquid phase exfoliation
CVD:	Chemical vapor deposition
R_H:	Hydrodynamic radius
d(H):	Hydrodynamic diameter
PDDF:	Pair distance distribution function
GIFT:	Generalized Indirect Fourier Transform
ORT:	Optimized regulation technique
DLVO:	Derjaguin, Landau, Verwey and Overbeek
rpm:	Rotations per minute

INTRODUCTION AND OBJECTIVE

Materials at a nanoscale size, which is approximately 1 to 100 nm in at least one dimension [1], are chemically more reactive, can change their properties and can become more effective then their larger sized counterparts. The reason for this is their relatively larger surface area to mass ratio on one hand; on the other hand, when materials are produced on the nanoscale, they gain interesting surface properties because of their active surface atoms that are not found within their large sized counterparts. Nanomaterials including carbon nanotubes, boron nitride nanotubes, graphene, boron nitride nanosheets, fullerene, metal nanowires, semiconductor quantum dots, inorganic nanoparticles such as gold and silver and so on are produced through various methods, which are divided into two groups, the top-down and bottom-up methods. The range of potential applications and the significance of nanotechnology and nanomaterials are growing rapidly.

One important branch of nanomaterials, which is becoming more and more desirable, is the group of the two-dimensional nanosheets. The motivation for studying 2D materials, investigating their properties, searching for new characteristics, which are not known yet, and researching potential applications, started with graphene about 13 years ago. Since its discovery in 2004 by Sir Andre Geim and Sir Konstantin Novoselov at the University of Manchester, for which they won a Nobel Prize in Physics in 2010 "for groundbreaking experiments regarding the two-dimensional material graphene" [2], these 2D materials have gained great worldwide attention. The interest is spreading rapidly also among other types of nanosheets, like for instance boron nitride nanosheets, which just like graphene, exhibit promising and fascinating properties. Scientists are very optimistic about this new group of nanomaterials and see great potential in them.

The atomically thin hexagonally arranged carbon crystal structure of graphene is an excellent candidate for various applications, due to its outstanding properties like strength, toughness, flexibility, transparence, and its very good thermal and electrical conductivity. These multifunctional properties of graphene open up opportunities that

have not yet been thought of, of using materials in completely different ways. Hence, graphene can have limitless applications. It can be used to make light weighted airplanes, trains, automobiles, spacecraft, durable batteries, flexible and semi-transparent electronics, transistors, medical scanners and bioelectric sensory devices. It can also be used in optoelectronics, computers, ultrafiltration, photovoltaic cells, and much more, even applications we haven't even thought about yet.

Another 2D material that is also playing an excellent role in the field of nanotechnology is hexagonal boron nitride nanosheets (denoted as *h*-BNNSs or just BNNSs). BNNSs are also known as "white graphene", because of their similar crystal structure. Hence, they have many similar properties, but differ in some of them; for example BNNS is an electrical insulator and thermal conductor, whereas graphene is both, an electrical and a thermal conductor. The extraordinary properties, such as high thermal and mechanical performance, high chemical and thermal stability, excellent lubricity, and strong insulating properties enable BNNSs to be applied as deep ultraviolet illuminants, dielectric gates, insulating thermal conductors, electronic coatings, anti-oxidation lubricants, and so on. As an electrical insulator with high thermal conductivity and remarkable chemical inertness, BNNSs possess more value than other conventional heat-transfer materials. It shows a great potential as thermal filler and is therefore an interesting candidate for the fabrication of thermally conductive and electrically insulating polymers. Wei-Li Song et al. demonstrate in their publication [3] in 2012 how BNNSs dispersed in polymer matrices give nanocomposite films with superior thermal transport performance, which shows the great potential of BNNSs in highly thermally conductive polymer nanocomposites.

However, since this is still a rather new field of research, there are many issues to be dealt with, and many questions to be answered. For instance, fabricating these nanosheets in large amounts still remains a big challenge, limiting their further research and applications in technology.

Jianfeng Shen et al. [4] could only achieve less than 1 % yield when using water and isopropanol at a 1 to 1 ratio and less than 0.86 % when using dimethylformamide (DMF) as solvent to exfoliate nanosheets from the bulk crystal in a sonication bath.

Chunyi Zhi et al. [5] reached around 0.1 % with DMF as solvent and the probe-type sonication method. Higher yields were achieved when using a water-alcohol mixture as solvent [6] or just pure water [7], with values up to 3 % and 5 %, respectively.

However, considering that around 0.5-1 % of a polymer is filler medium, these yields are still too low. The demand for large amounts on BNNSs, especially additive- and solvent-free for polymers, is increasing rapidly.

Finding an improved, cost-effective and fast method on how to prepare high amounts on these 2D materials is therefore of great importance. This thesis focuses on the high-yield production and characterization of boron nitride nanosheets. Since these sheets should be solvent-free for their integration in polymers, methods on how to remove the solvent, without an occurring aggregation, were also investigated. The aim is to prepare defect-free, additive-free, dried (meaning, they are not dispersed in a solvent) boron nitride nanosheets in high amounts and in a fast, environmental friendly and cost-effective way, preferably in their monolayer, or just a few-layer form, which are stable for long periods of time, without irreversibly aggregating.

There are yet many challenges to overcome, but researchers all around the world are fascinated with these materials and are working untiringly on understanding them and finding a way on how to manufacture them. When this breakthrough is achieved, 2D materials will have the potential to revolutionize the technology. That, which is known only as science fiction and theory until now, will be made reality and practice. This will be the beginning of a new and fascinating area in science and technology.

CHAPTER 1

Theoretical background

1.1. Introduction to two-dimensional materials

Two-dimensional (2D) materials, also called single layered materials or two-dimensional (2D) nanosheets are materials consisting of a single or just a few layers of atoms. These materials have gained worldwide attention in recent years because of their outstanding properties due to their structure and dimensionality. They were believed to exist only in theory because of their thermodynamic instability due to thermal fluctuations in low-dimensional crystal structures. [4-6] This changed in 2004, when Novoselov and Geim exfoliated and isolated the first single layer of graphene from graphite using the mechanical cleavage method. [7] This made it possible for them to explore the amazing physical, optical and electrical properties of graphene, which raised an interest to also explore other 2D nanomaterials that posses similar layered structures but different properties, such as hexagonal boron nitride nanosheets (*h*-BNNSs) [8], transition metal dichalcogenides (TMDs; like MoS_2, TiS_2, TaS_2, WS_2, $MoSe_2$ etc.) [9-12], graphitic carbon nitride (g-C_3N_4) [13], layered metal oxides [14], and layered double hydroxides (LDHs) [15]. The unique properties of 2D materials differ from those of other types of nanomaterials, such as zero-dimensional (0D) nanoparticles, like fullerene, one-dimensional (1D) nanowires or nanotubes, and three-dimensional (3D) networks, as well as from their bulk counterparts. Some ultrathin 2D materials, especially monolayer nanosheets e.g. graphene, possess extraordinary electronic and thermal properties. [16] They also possess high optical transparency and mechanical flexibility because of their atomic scale thickness, which makes them great candidates for applications in highly transparent and flexible optoelectronic or electronic devices. [16] The 2D nanomaterials have become an important class of materials in chemistry, condensed mater physics and material science and their interest is growing drastically with thousands of research papers being published every year. A large number of synthetic methods, such as mechanical cleavage [17-19], liquid exfoliation [20-24], ion-intercalation and exfoliation [25-28], anion exchange and exfoliation [29, 30], chemical vapor deposition growth (CVD) [31-33], wet-chemical syntheses [34-36], etc. have been developed for the preparation of these materials. Two-dimensional nanosheets are promising for a variety of applications such as electronics and optoelectronics [16, 37-39], catalysis [40-42], energy storage and conversion [43-47], biomedicine [48-50], sensors [51-55] and so on.

1.2. Graphene

Graphene is the first two-dimensional material, discovered in 2004 by Sir Andre Geim and Sir Konstantin Novoselov. [56] It consists of carbon atoms hexagonally arranged into a two-dimensional (2D) honeycomb lattice, where the C-C bond is sp^2 hybridized, and each carbon atom provides a non-bonding electron to form a π bond cloud, allowing the electrons to move freely between the layers. [57]

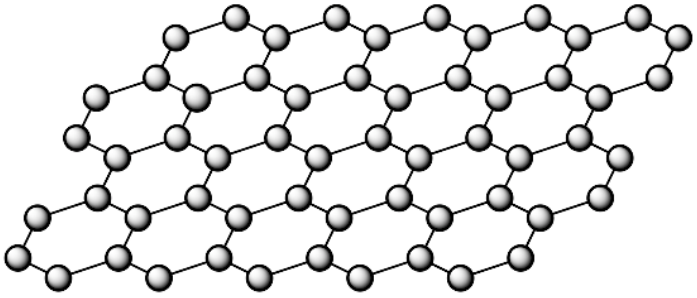

Figure 1: A layer of graphene, consisting of carbon atoms hexagonally arranged into a two-dimensional honeycomb lattice.

The hexagonal geometry makes graphene very stable. [58] The length of the C-C bond is around 0.142 nm and the thickness of the layer is 0.35 nm. [57] Graphene is a basic building block for graphitic materials of all other dimensionalities, such as 0D fullerenes, 1D nanotubes or 3D graphite. [16] (Fig. 2)

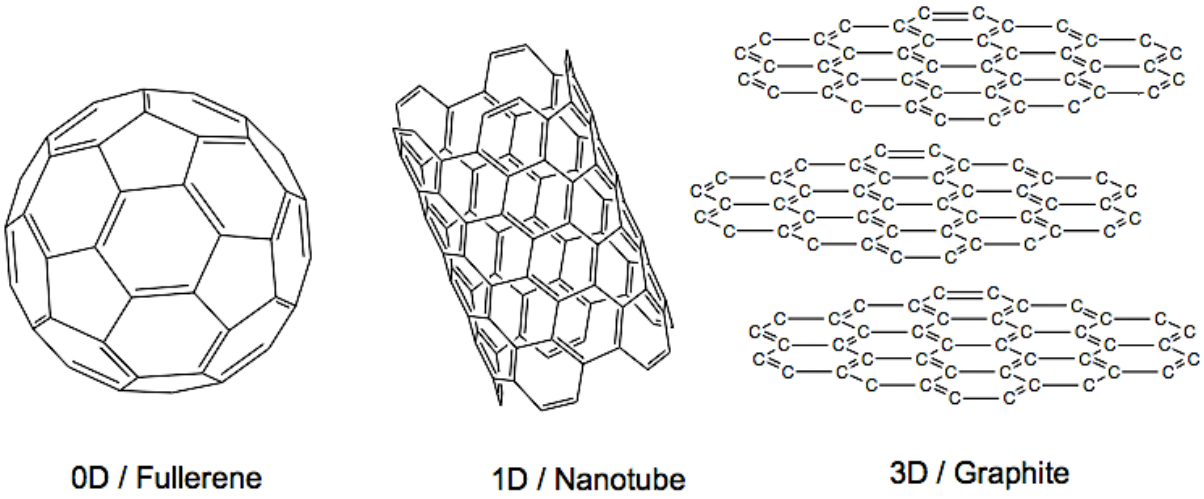

Figure 2: Graphitic materials of different dimensionalities: 0D fullerene, 1D nanotube, 3D graphite.

Graphene was believed to be thermodynamically unstable and that the atomic monolayer would roll or fold. The contrary was proved in 2004 by Geim and Novoselov [56] and since then graphene and other 2D materials have gained great interest.

It is the thinnest and hardest nanomaterial [59] with a tensile strength of 125 GPa, an elastic modulus of 1.1 TPa and a 2D ultimate plane strength of 42 N m^{-2}. Graphene's carrier mobility is 2 x 10^5 cm^2 (V^{-1} s^{-1}) [60, 61], which is 140 times the value of silicon [57] and is only affected by impurities and defects. It has a thermal conductivity of up to 5.5 x 10^3 W (m^{-1} K^{-1}) [62, 63] and the electrical conductivity can reach 10^6 S m^{-1}, meaning graphene has the best conductivity among known materials at room temperature. [57] That is because it is a zero-band-gab semiconductor and the electron in graphene is a type of massless Dirac Fermion. [64] This unique band configuration of the Dirac point allows electrons in graphene to pass through the barriers with 100 % probability. [65] Theoretically, graphene's specific surface area is up to 2630 m^2 g^{-1}. For a single layer, the absorption and transmittance of visible light are 2.3 % and 97.7 %, respectively. [66, 67]

These extraordinary properties allow this nanomaterial to be widely applied in many areas of nanoelectronic devices, spin electronics, energy storage, thermal conductivity materials, composites and coatings, membranes, sensors and medicine.

1.3. Boron nitride

Boron nitride is an inorganic compound with a wide range of applications like surface coatings, ceramic composites, electrical insulators, lubricants etc. because of its unique properties including chemical inertness, high oxidation resistance, excellent lubricity, high thermal conductivity, good electrical insulation, non-toxicity and environmental friendliness. [68,69]

It has a chemical formula BN and consists of equal numbers of boron and nitrogen atoms. It can be found in several crystalline forms, depending on the hybridization of the orbitals, which can be either sp^2 or sp^3 hybridized. sp^2 hybridized bonding forms

hexagonal (*h*) and rhombohedral (*r*) lattices, whereas sp^3 hybridized bonding forms cubic (*c*) or wurtzite (*w*) lattices. *h*-BN (also called *α*-BN) [70] has the most stable structure and is widely available. (Fig. 3)

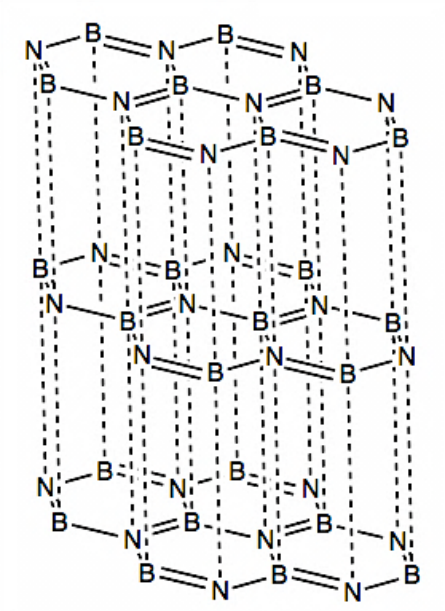

Figure 3: Layered structure of hexagonal boron nitride. Boron and nitrogen atoms are sp^2 hybridized and the layers are held together by weak van der Waals forces.

The atoms are sp^2 hybridized and the multiple two-dimensional (2-D) BN layers are stacked together by weak van der Waals forces. [71] *h*-BN is often referred to as "white graphite" due to its similar bonding and structure to graphite. [72] (Fig. 4)

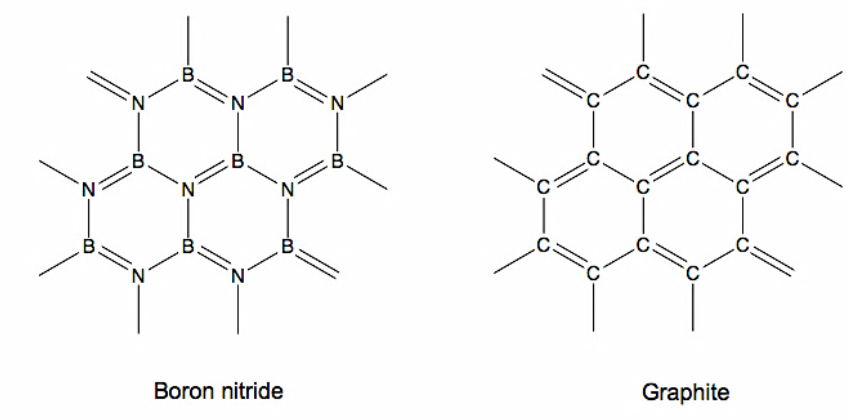

Figure 4: Boron nitride is often called "white graphite" due to structure similarity to graphite. In both cases, the atoms are sp^2 hybridized and hexagonally arranged. Boron nitride consists of alternating boron and nitrogen atoms, whereas graphite consists of only carbon atoms.

The lattice constants for boron nitride are $a_0 = b_0 = 2.50 - 2.51$ Å (which is the distance between the centers of neighboring hexagonal rings) and $c_0 = 6.66 - 6.67$ Å (which is the height of two sheets); these are very similar to those of graphite: $a_0 = 2.5$ Å and $c_0 = 6.7$ Å. [72]

Hexagonal rings form basal planes, where every B atom bonds to three N atoms in the plane and every N atom bonds to three B atoms. The B-N bond in the basal plane is extremely strong; stronger than the C-C bond in diamond or the B-N bond in *c*-BN. [73] The covalent B-N bonds are 1.45 Å in length and the distance between the layers held by van der Waals forces is 3.33 Å. [74]

The polarity of the B-N bond is responsible for the buildup of effective charges on the atomic centers. Therefore, the interlayer electrostatic interactions between partially charged atoms should play a role in the interlayer binding, which would result in a somewhat shorter interlayer distance than that measured for graphite. [75] Nevertheless, the interlayer distance in *h*-BN and graphite is comparable, suggesting that electrostatic interactions have little effect on the interlayer binding. [75] Another study [76] shows also that the van der Waals forces are mainly responsible for the fixed distance between the layers, whereas the electrostatic forces dictate the optimal stacking mode, which is demonstrated in figure 5.

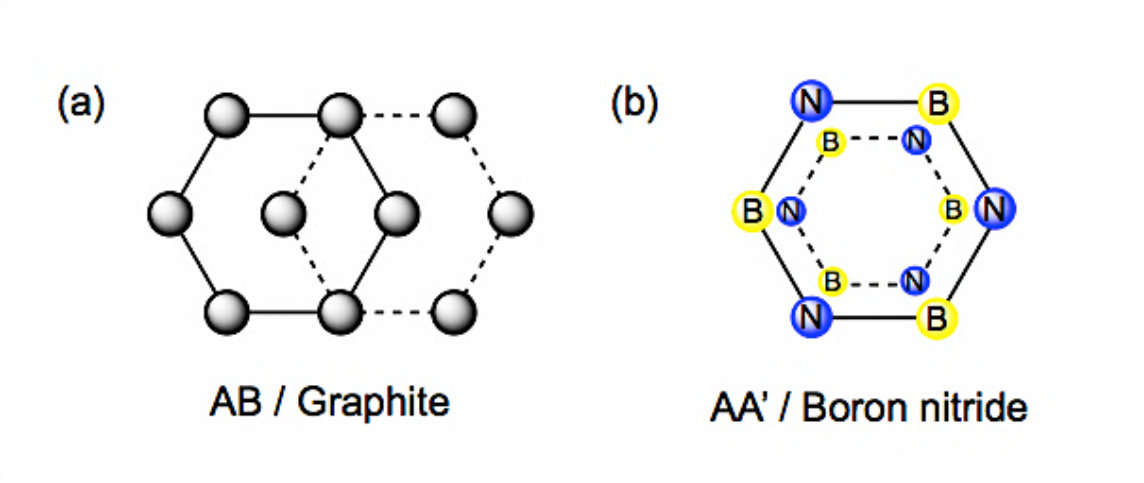

Figure 5: Stacking modes in hexagonal lattices: (a) graphite, where a carbon atom resides atop the center of a hexagon of the neighboring layer; (b) h-BN, where a nitrogen atom resides atop a boron atom of the adjacent layer.

Figure 5a shows an optimal AB stacking of graphite, where a carbon atom in a certain layer resides atop the center of a hexagon of the neighboring layer. [75] In the case of *h*-BN (Fig. 5b), a partially negatively charged nitrogen atom in one layer resides atop of a partially positively charged boron atom of the adjacent layer, also called AA' stacking mode. [75]

Hexagonal boron nitride is an electrical insulator and has a direct-band-gap energy of 5.971 eV. [77] It has been used as an ultraviolet light emitter due to its large absorption of light in the far ultraviolet region. [77] A far-ultraviolet plane-emission handheld device based on the absorption property of hexagonal boron nitride was demonstrated. [78] In addition to that, it has sliding properties, because of its layered structure, and has a low coefficient of friction, and is therefore used as a mold releasing powder and parting agent in the foundry industry. [79] *h*-BN powder can also be used as a "dry lubricant", because it doesn't lose its lubricant property in either sub-zero nor high-temperature environments; that is why it can be used as a dry lubricating agent in spaceships and satellites. [79] Due to its good dispersion, sliding behavior, oil absorption capability, transparency under visible light and good thermal conductivity, *h*-BN is being widely used in the cosmetic industry, for example in forms of makeups like mascara, lipstick, makeup pencils, etc. [79]

Hexagonal boron nitride has high-temperature oxidation resistance up to 800°C in air and is quite stable up to 2400°C in nitrogen atmosphere. [80] Due to its high-temperature oxidation resistance and non-wet ability, thanks to its chemical inertness and very limited surface activity, *h*-BN is extensively used in high-temperature refractory applications, such as furnace, coatings etc. [79]

1.4. Hexagonal boron nitride nanosheets (BNNSs)

Analogous to graphite, *h*-BN has a honeycomb structure but with alternating boron and nitrogen atoms, instead of carbon atoms, linked by a sp^2 hybridized strong covalent bond. The B-N bonds have an ionic character and are 0.144 nm (0.142 nm in graphene) in length and the distance between the centers of adjacent hexagonal rings is 0.25 nm (0.246 nm in graphene). [74]

The interlayers of *h*-BN are held by weak van der Waals forces. [71]

Figure 6 shows the structural similarities between graphite and boron nitride.

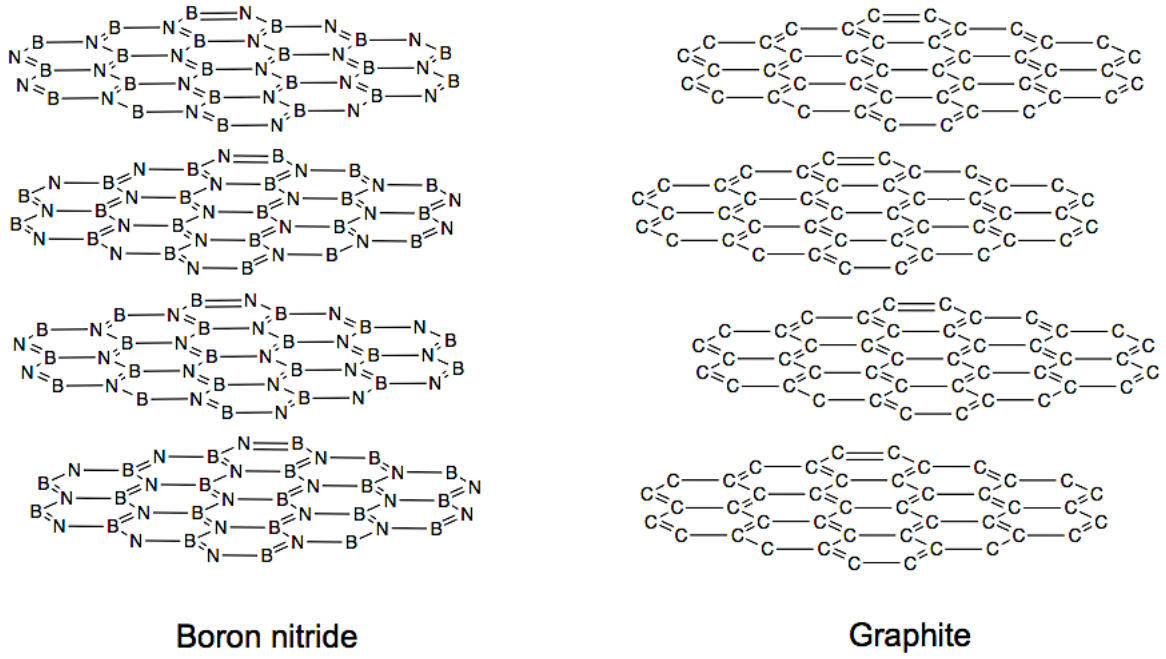

Figure 6: Structural similarities between boron nitride and graphite. The layers are held together by van der Waals forces. In graphite, a carbon atom resides atop the center of the hexagon of the neighboring layer, whereas in h-BN, a nitrogen atom resides atop a boron atom of the adjacent layer.

There is a difference in the stacking sequence between boron nitride and graphite. Boron nitride has an AA' stacking, where boron atoms reside on top of nitrogen atoms, while graphite possesses a AB stacking sequence, as explained in chapter 1.3.

The difference in electronegativity of boron and nitrogen atoms leads to partial ionicity of the B-N bonds. As a result, chemical bonds form as bridges between the atoms of neighboring layers, which is usually known as "lip–lip" interactions. [81-84]

Just like graphene, BNNS is also a basic building block for other low-dimensional BN nanostructures. [85]

The BNNS has a band gap of 6.0 eV. [86, 87] The calculated Young's modulus of one-layered BN is 0.71 - 0.97 TPa, and the breaking strength is 120 - 165 GPa. [88-91] These values are close to the experimental values of graphene (Young's modulus of 1.0 TPa and breaking strength of 130 GPa).[59] The thermal conductivity of few-layer boron nitride was measured to be 100 - 270 W (m^{-1} K^{-1}), [92-94] making them one of the best electrically insulating thermal conductors. 2D *h*-BN has no absorption in the visible range, but has absorption spectroscopy in the ultraviolet and deep ultraviolet region and a good photoluminescence property. [57] BNNSs have a strong resistance to oxidation and can withstand temperatures up to 800°C, in contrast to that of graphene at 400°C. [95] Hence, there are suitable for applications at high temperature and for manufacturing processes that require heating temperatures. The higher thermal stability and excellent impermeability of BN nanosheets make them preferable to graphene in protecting metals from oxidation and corrosion. [96]

Boron nitride nanosheets offer many unique properties and can be applied widely. However, finding an improved, less toxic and environmental friendly way to fabricate BNNSs of high quality in high yields still remains a big challenge.

1.5. Preparation of two-dimensional materials

Many synthetic strategies to produce ultrathin 2D nanomaterials have been developed, such as mechanical cleavage, liquid phase exfoliation, ion-intercalation and exfoliation, ball milling, chemical vapor deposition (CVD) and wet-chemical synthesis. These methods can be generally classified into two categories: top-down (mechanical cleavage, exfoliation, ball milling) and bottom up approaches (CVD, wet-chemical). [97]

The top-down method relies on the exfoliation of layered bulk crystals into single- or few-layer nanosheets, in which different driving forces, such as ultrasound or shearing forces, are used to break the weak van der Waals interaction between the layers. The bottom-up method is the direct synthesis of 2D nanomaterials from different precursors *via* chemical reactions at given experimental conditions. [97]

1.5.1. Top – down method

Mechanical Cleavage

The mechanical cleavage is the first exfoliation method Geim and Novoselov used to isolate the first 2D sheet of graphene from a bulk of graphite in 2004. [17-19, 56, 98] They used Scotch tape to peel off flakes of graphene from the bulk crystal of graphite. Another piece of Scotch tape is adhered onto the first one, where the flakes of graphene are, and both tapes are then detached from one another, separating the graphene layers from each other. This process was repeated several times until very thin flakes were obtained. Then, the Scotch tape with the thin flake is applied to a target substrate (e.g. SiO_2/Si) under gentle pressure. Afterwards, the Scotch tape is peeled off from the substrate and single- or few-layer graphene can be characterized by using an optical microscope. [97]

This method was later used for other 2D crystals, including *h*-BNNS, MoS_2, $NbSe_2$ and $Bi_2Sr_2CaCu_2O_x$. [17] Many other types of single- or few-layer nanosheets have been prepared, such as other 2D transition metal dichalcogenides TMDs (TiS_2, TaS_2, WS_2, WSe_2, $TaSe_2$, etc.), metal oxides, black phosphorus (BP), metal organic frameworks (MOFs), and so on. [18, 19, 98-100]

The 2D materials prepared with this process remain in the same crystal structures as their bulk crystals, because there are no chemical reactions used. As a result the ultrathin nanosheets possess excellent crystal quality with very few defects, and are therefore ideal for the study of their properties and the demonstration of the electronic devices. [97]

There are however some limitations, like the quite low yield, the necessity of a substrate to support the produced nanosheets and the difficulty to control the thickness, size and shape of the obtained 2D nanomaterials. [97] It is necessary to improve the production rate and the yield in order to meet the large quantities that are needed for commercialization and for practical applications. [97]

Liquid Phase Exfoliation

Liquid phase exfoliation (LPE) is a typical strategy that is used widely to exfoliate layered bulk crystals to thin nanosheets. [20-24, 101] In this method, the bulk crystals are exfoliated directly in solvents, e.g. N-methyl-2-pyrrolidone (NMP), dimethylformamide (DMF), acetone, acetonitrile (ACN), isopropanol (IPA) etc. *via* sonication or shear mixing. [20] The sonication, or the shearing force, can destroy the weak van der Waals interaction between layers, but it cannot break the strong covalent bonds in each layer. Good matching of the surface tension between the layered crystal and the solvent is significant for minimizing the energy and increasing the efficiency of the exfoliation. [4] The solvent is also important in stabilizing the exfoliated sheets and preventing their aggregation. [4]

The sonication in aqueous polymer or surfactant solution improves exfoliation, because these additives can also stabilize the exfoliated sheets. [20] Many ultrathin 2D nanomaterials, including graphene, *h*-BNNS, TMDs (MoS_2, WS_2, $MoSe_2$, $NbSe_2$, $TaSe_2$, $NiTe_2$, and $MoTe_2$), metal oxides (e.g., WO_3), metal hydroxides, MOFs, BP, have been prepared by this method from their layered bulk crystals. [20-24, 101]

The yields produced with this method are higher than with other methods, making this promising for commercial applications. However, the yield of single-layer nanosheets, as well as the final concentration of nanosheets in solvent, is still quite low; the lateral sizes of the sheets are relatively small, and most of the organic solvents that are used are toxic. [97] Even though this method seems very promising, there is still some room for improvement. [97]

Ion – intercalation and exfoliation

This method relies on the intercalation of ions between the layers of the bulk crystal to weaken the van der Waals forces. The intercalated compounds are then exfoliated to single- or few-layer nanosheets by using sonication. [25-28, 102-104] The most used intercalators are organometal compounds, such as butyllithium and metal naphthalenide (metal=Li, Na, K). [102-104] The bulk crystals are simply immersed or refluxed in the intercalator solution and then the nanosheets can be obtained by sonication of the ion-intercalated compounds in water or ethanol. [97]

This method also seems promising, but there are however some challenges to overcome. The process requires high temperatures, up to 100°C, and long reaction days, up to 3 days. [102, 103] Also the organometal compounds are very sensitive to oxygen and water, and become highly explosive when exposed to them. [26, 27]

Ball milling

In ball milling process, shearing forces are used to exfoliate the nanosheets from the bulk crystal. [105, 106] Direct contact of the *h*-BN powders with the grinding balls can be avoided by adding a solvent, which improves the efficiency of the process and the quality of the nanosheets. [105] Ball milling without using a solvent creates a large number of defects and impurities in the nanosheets. [107-109]

1.5.2. Bottom – up method

Chemical vapor deposition

The chemical vapor deposition (CVD) method is a bottom-up method, which is used to produce 2D nanosheets on substrates. [31-33, 110, 111] The precursors react on the surface of a substrate to form ultrathin 2D flakes or large-area ultrathin films, when exposed to it at high temperature and high vacuum. [97] This method has been successfully used to prepare graphene, TMDs (MoS_2, WS_2, $MoSe_2$, WSe_2, ReS_2, GaS_2, etc.), BNNSs, topological insulators (e.g. In_2Se_3 and Bi_2Se_3), and metal oxides. [31-33, 110, 111] Chemical vapor deposition also faces a few challenges, such as the fact that CVD growth process needs high temperature, high vacuum, and a specific substrate to support the grown ultrathin 2D nanosheets. [97] A transfer process to move the nanosheets onto desired substrates for further research and applications is required as well. [97]

Wet – chemical synthesis

Wet-chemical synthesis is another bottom-up method that has been used to prepare 2D nanomaterials. [34-36, 112, 113] Materials are synthesized from certain precursors *via* chemical reactions in solution.

Surfactants are added, in order to control size, shape and morphology of the materials, as well as to stabilize them. [97]

Some of these methods include template synthesis, hydro/solvothermal synthesis, self-assembly of nanocrystals and soft colloidal synthesis. [97] It is possible to produce higher yields of nanomaterials with this method; yet, it is hard to obtain single-layer nanosheets, because the synthesis is lightly affected by reaction parameters, such as temperature, reaction time, concentration of precursors and solvent. [97]

Even though some general methods on how to produce two-dimensional nanomaterials exist and have been successfully performed, there is still a lot to improve. To this day, fabricating 2D nanosheets in high yields, enough to be applied widely in the industry and technology, still remains a challenge.

1.6. Characterization of two-dimensional materials

The methods that were used to characterize and to distinguish the size, thickness and shape of the BNNSs are ultraviolet-visible spectroscopy (UV-Vis), dynamic light scattering (DLS), small angle X-ray scattering (SAXS), and transmission electron microscope (TEM).

Ultraviolet – visible spectroscopy (UV – Vis)

The UV-Vis spectroscopy is an absorption spectroscopy in the ultraviolet and visible region and is based on the Lambert – Beer law.

$$A = \log_{10} (I_0/I) = \varepsilon\, c\, d \qquad (1)$$

A is the measured absorbance, $\mathbf{I_0}$ the intensity of the light before it passes through the sample, **I** is the intensity of light passing through a sample and the ratio $\mathbf{I_0/I}$ is called the transmittance. **ε** is the extinction coefficient, which is an intrinsic property of the species being measured; **c** is the concentration and **d** the width of the cuvette. The absorption of boron nitride nanosheets is in the ultraviolet range and the extinction coefficient at a wavelength of 300 nm is 2354 L / (g m). [4]

The concentration of the boron nitride nanosheets in the sample was calculated using the Lamber – Beer law after measuring the absorbance *via* UV-Vis spectrometer.

Dynamic light scattering (DLS)

Dynamic light scattering (DLS), also referred to as photo correlation spectroscopy (PCS) or quasi-elastic light scattering (QELS) is a technique, which is used to obtain the average size of Brownian nanoparticles that are dispersed at a given temperature and viscosity. [114]

DLS measures the Brownian motion, which is the random movement of the particles due to the bombardment by the solvent molecules that surround them, and relates this to the size of the particles. The velocity of the Brownian motion is defined by the diffusion coefficient D ($m^2\ s^{-1}$), and is depended on the solvent viscosity and the temperature.

The hydrodynamic radius R_H of the particles is calculated from the diffusion coefficient D by using the Stokes-Einstein equation: [114]

$$d(H) = \frac{k_B T}{3\pi\eta D} = 2 * R_H \qquad (2)$$

, where:

d(H) = hydrodynamic diameter (m)

R_H = hydrodynamic radius (m)

D = diffusion coefficient ($m^2\ s^{-1}$)

k_B = Boltzmann's constant ($1.38064852 \times 10^{-23}$ J K^{-1})

T = absolute temperature (K)

η = viscosity of the solvent (kg s^{-1} m^{-1})

The hydrodynamic radius is a value that refers to how a particle diffuses within a solvent and differs from the lateral diameter or the lateral radii of the particle. The lateral radii can be calculated from the resulting hydrodynamic radii. [115]

The lateral radius of oblate ellipsoids is calculated using the thicknesses obtained from the SAXS evaluation: [116]

$$R_H = a/G\left(b/a\right) \qquad G\left(b/a\right) = \frac{\operatorname{atan}\left(\sqrt{\left(b/a\right)^2 - 1}\right)}{\sqrt{\left(b/a\right)^2 - 1}} \tag{3}$$

, where:

b = the long semiaxis (lateral radius)

a = the short semiaxis (half thickness)

R_H = the hydrodynamic radius of the ellipsoid.

An example is demonstrated in Figure 7 [115], where the main thickness of the particles (5 nm) was used to obtain the resulted lateral radius distribution.

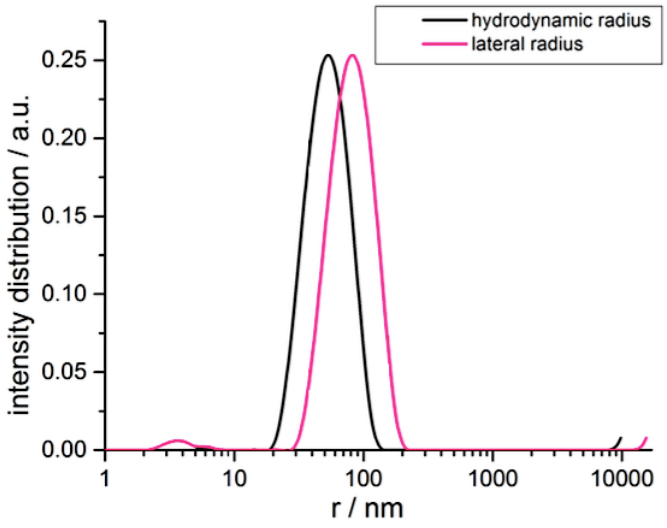

Figure 7: Hydrodynamic and lateral radius of MoS_2 nanosheets. [115]

Small angle X – ray scattering (SAXS)

Small angle X-ray scattering (SAXS) is a nanoscale characterization technique to study material structures at large distances, or small angles. [117] It is based on the interactions of an X-ray beam with the electrons in the sample. [118]

SAXS measurements can be performed to determine the thickness of the nanosheets by using the pair distance distribution function (PDDF) of the thickness $p_t(r)$, which, in case of planer particles, is given as: [119]

$$p_t(r) = (1/\pi) \int_0^{\alpha} I_t(q) \cos(qr)\, dq \qquad (4)$$

, where:

$I_t(q)$ = cross-section scattering function [120]

q = the magnitude of the scattering vector defined by:

$$q = (4\pi/\lambda_0) \sin \theta \qquad (5)$$

, where:

2θ = the scattering angle

λ_0 = the wavelength of the monochromatic radiation.

The $p_t(r)$ function is calculated using the GIFT (Generalized Indirect Fourier Transform) program. The theoretical shape of the pair distance distribution function of nanosheets with a lamellar structure is a triangle, as shown in figure 8. [115] The distribution of thicknesses of the nanosheets is fitted by a sum of triangular functions, which correspond to sheets with thicknesses of 5-25 nm (Fig. 9). [115]

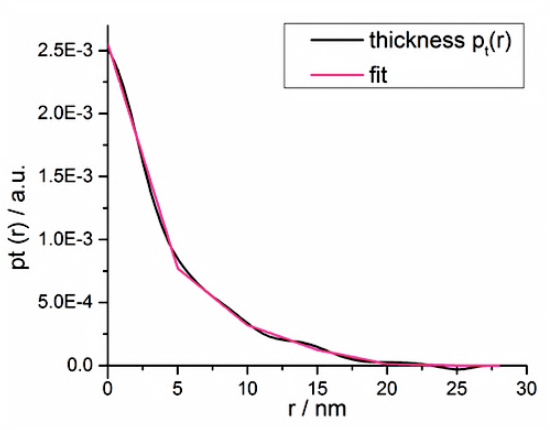

Figure 8: $p_t(r)$ of MoS_2 nanosheets fitted with a distribution of 5 thicknesses. [115]

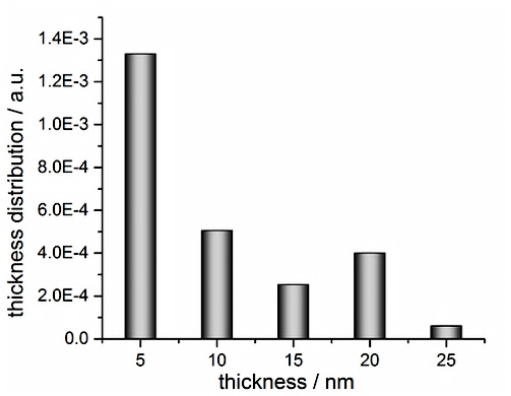

Figure 9: Distribution of thicknesses of MoS_2 nanosheets. [115]

The flat shape of the nanosheets can also be determined using SAXS. The scattering curve of planar objects can be separated into the planar factor I_{plane} and a thickness factor $I_t(q)$: [115]

$$I(q) = I_{plane} * I_t(q) = \frac{2\pi * A}{q^2} * I_t(q) \qquad (6)$$

, where **A** is the area of the lamella.

By plotting lg(I) vs lg(q) (Fig. 10) a slope of -2 at low scattering angles confirms the platelet shape of the nanosheets measured. [115]

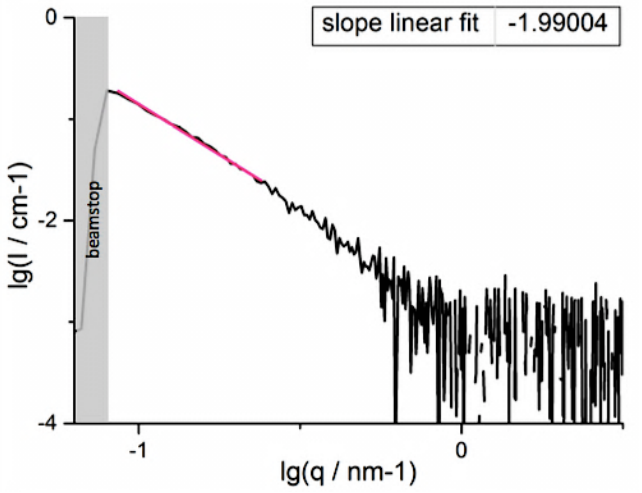

Figure 10: X-ray scattering curve of a dispersion of MoS_2 nanosheets. [115]

Transmission electron microscopy (TEM)

The transmission electron microscopy TEM is a widely used method for the characterization of materials down to the atomic scale. [121]

The small de Broglie wavelength of the electrons that travel at a significant fraction of the speed of light enables the high three-dimensional resolution that is achieved in a transmission electron microscope. [122] This makes it possible to get a resolution a thousand times better than with a light microscope. Hence, TEM is used to obtain information about the shape of the nanosheets.

1.7. Colloids [123]

A colloid, or dispersed phase, is a dispersion of small particles, meaning less than about 500 nm in diameter, of one material in another. Colloidal particles are mostly aggregates of numerous atoms or molecules, however they are too small to be seen with an ordinary microscope. The name of a colloidal dispersion depends on the two phases involved. An aerosol is dispersed solid particles in gas such as smoke or liquid in gas like fog and many sprays; sols are solid particles in liquid, such as clusters of gold atoms in water or solid in solid such as ruby glass, which is a gold-in-glass sol and achieves its color by scattering. Emulsions are liquid particles in a liquid, like milk or mayonnaise, which is oil in water; and gels are liquid particles in solid, like gelatin, which is protein in water. Another classification of colloids is as lyophilic, or solvent-attracting, and lyophobic, solvent - repelling. If the solvent is water, then the terms hydrophilic and hydrophobic are used instead.

The electrical double layer [123]

Colloids are thermodynamically instable but kinetically inert. One of the reasons of kinetic stability is the presence of an electric charge on the surfaces of the particles. There are two regions of charges; first there is a rather immobile layer of ions that adhere strongly to the surface of the colloidal particle. The radius of this sphere, which determines the mobility of the particles, is called the radius of shear.

The electrical potential at the radius of the shear is called zeta potential ζ and is relative to its value in the distant, bulk medium. Second, this charged unit attracts an atmosphere of mobile ions, which is oppositely charged. The inner layer of charge and the outer ionic cloud form the electrical double layer.

DLVO Theory

Derjaguin, Landau, Verwey and Overbeek (DLVO) developed a theory of colloidal stability, which helps understand interactions between colloidal particles and their aggregation behavior. The principle ideas were first developed by Boris Derjaguin [124], and then enhanced in an article together with Lev Landau [125] and later, they were publicized in a book by Evert Verwey and Jan Overbeek [126]. In DLVO theory, the two determining interactions for the stability of a colloidal system are the attractive van der Waals interactions between the colloidal particles, and the repulsive electrostatic Coulomb interactions, which is the repulsive interaction between the charges of the electrical double layers on neighboring particles. *[123]*

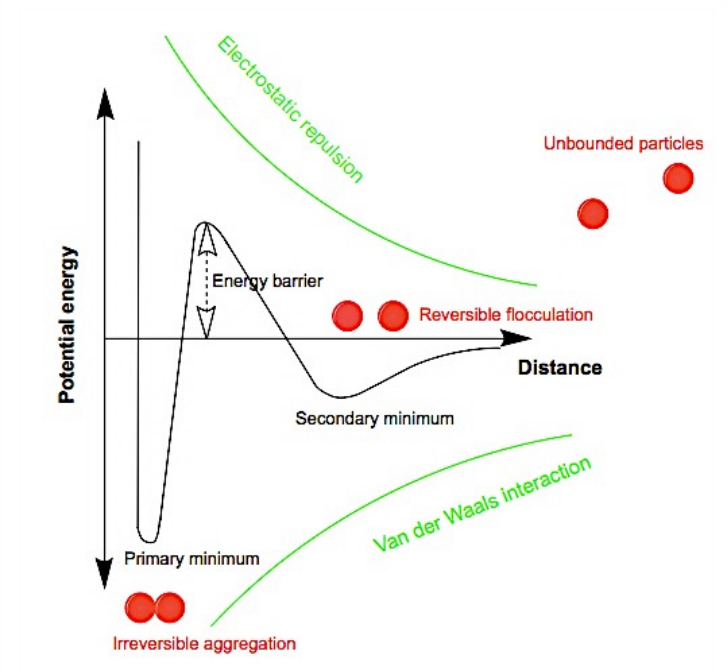

Figure 11: Depending on the distance between the particles, the potential energy of their interaction varies. Flocculation, which is the reversible aggregation of the colloidal particles, occurs at the secondary minimum, whereas the irreversible aggregation, also called coagulation, occurs at the primary minimum, where the potential energy is at its lowest point. At this point, the distance between the particles is so small, that the attractive van der Waals forces predominate.

When the ionic atmosphere is dense, the potential energy falls into a secondary minimum, where there is not enough electrostatic repulsion to prevent two colloid particles from coming closely together. As a result, flocculation, the aggregation of the colloidal particles, occurs. Flocculation is mostly reversible, and the flocculated material can often be re-dispersed by agitation. Coagulation, the irreversible collapse of the colloid into a bulk phase, occurs when the separation of the particles is so small that the attractive van der Waals forces predominate, and they enter the primary minimum of the potential energy curve. [123,127]

Surface tension [127]

The imbalance of forces is responsible for the smooth surface of stationary liquids; a molecule in the inside of a bulk experiences attractions from all directions, whereas those at the surface experience only inward forces. A molecule at the surface has a higher potential energy than one in the bulk because it interacts with fewer neighbors, therefore work must be done, in order to bring a molecule from the bulk into the surface layer. The work, required to increase the area of surface by $\Delta\sigma$, can be given as $w = \gamma\Delta\sigma$, and is proportional to that area. The constant of proportionality γ is called the surface tension. The surface tension of a solvent is an important parameter in the exfoliation and dispersion process of nanosheets. [128]

CHAPTER 2

Results and discussion

Boron nitride nanosheets have the ability to improve the thermal conductivity of polymer-based composites. However, investigating the effects of these 2D materials on polymers, as well as the properties of these polymers, containing the nanosheets, requires high amounts on BNNSs. A cost-effective and fast preparation of BNNSs is of great significance, and is what triggered motivation for this work.

The liquid phase exfoliation was chosen for the preparation of BNNSs, because it is a more suitable method for the production of high yield nanosheets, and it can be scaled up. In order to improve the LPE method, the effect of different solvents on the exfoliation of the sheets, as well as the yield and size of the BNNSs prepared by bath- and probe-type sonication, were investigated. Since the BNNSs should be as pure as possible, for their integration in polymers, there were no surfactants used. Furthermore, it was shown that the non-exfoliated boron nitride could be recycled, a process, which leads to low final yields of the nanosheets. Therefore, reducing and removing the solvent without the occurrence of aggregation was also studied.

This work presents an improved LPE method for the preparation of approximately 1 g of BNNSs in just a few days.

The nanosheets were characterized successfully by UV-Vis, DLS, SAXS and TEM.

2.1. Solvent

The liquid phase exfoliation of boron nitride nanosheets from the *h*-BN bulk crystal was performed in different solvents, shown in the following table. (Tab. 1)

Solvent	Yield / %
Isopropanol (IPA)	0.27 - 0.30
N-methyl-2-pyrrolidone (NMP)	0.10 - 0.12
Polyethylenglycol$_{200}$ (PEG$_{200}$)	0.07 - 0.09
Acetonitrile (ACN)	0.13 - 0.15
Acetone	-

Table 1: Solvents that were used for the liquid phase exfoliation.

According to Jianfeng Shen et al. [4], matching the ratio of polar components to dispersive components of surface tension of the solvent to that of the 2D material leads to efficient exfoliation of the nanosheets and to stabilization of the 2D sheets after exfoliation. The surface tension components of the solvents used for the exfoliation are summed up in the following table (Tab. 2). [4]

Solvent	Dispersive component	Polar component	Polar component / dispersive component
IPA	19.50	3.50	0.179
NMP	29.21	11.58	0.396
PEG_{200}	29.90	13.60	0.455
ACN	8.80	19.30	2.193
Acetone	16.50	6.80	0.412

Table 2: Surface tension components of solvents. [4]

The ratio of polar to dispersive component of the 2D *h*-BN is 0.450. [4] According to this information, PEG_{200} should have been the best choice of a solvent for the liquid phase exfoliation. However, the obtained yields (Tab. 1) show that isopropanol is more suitable for the exfoliation of the nanosheets from the bulk crystal.

A reason for this could be a combination of its polarity and the small size of its molecules. Polar solvents get strongly adsorbed on the surfaces and in between *h*-BN layers forming “quasi-stable” states through electrostatic interactions, which reduce interlayer binding and favor exfoliation. [129]

NMP and ACN also show some good results, but their high toxicity makes them unfavorable for the probe-type sonication method, where the sample stays open during the sonication process. Acetone showed no results at all.

The size distribution of the exfoliated BNNSs was measured by DLS. (Fig. 12)

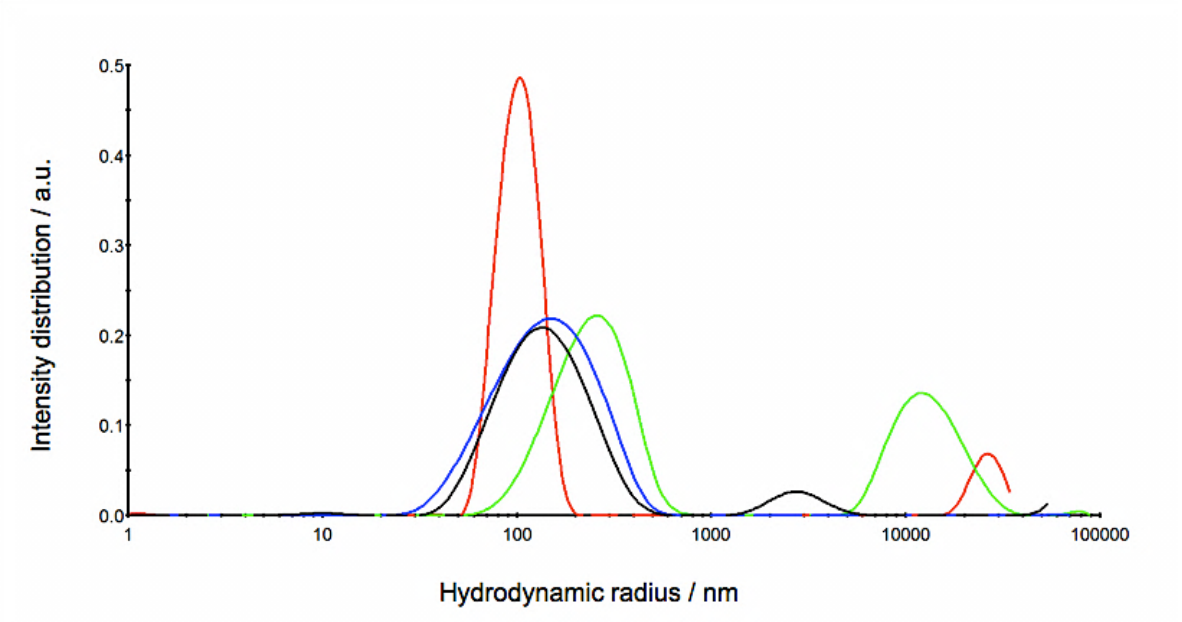

Figure 12: Influence of different solvents on the hydrodynamic radii of BNNSs prepared by exfoliation in a bath sonicator for 2h; IPA=red; PEG_{200}=green; NMP=blue; Acetone=black.

The hydrodynamic radius of BNNSs in isopropanol is about 100 nm. Since the highest yield of BNNSs is achieved in isopropanol, which is a rather non-toxic solvent, in comparison to the others, the decision was made to perform the upcoming experiments in this solvent.

2.2. Method

Both, bath and probe-type sonication have been used for the liquid phase exfoliation.

Since the ultrasonic intensity distribution in ultrasonic bath is not homogeneous, an aluminium foil test was performed to determine where the hot spots in the bath are. [130, 131] A sheet of aluminium foil was dipped into the water of the ultrasonic bath and was sonicated for about 1 minute. The maximum intensity is where the foil is mostly perforated (Fig. 13). [130, 131] The vessel containing the *h*-BN bulk crystals in solvent to be exfoliated was placed at the hot spot, where the maximum exfoliation effect can be achieved.

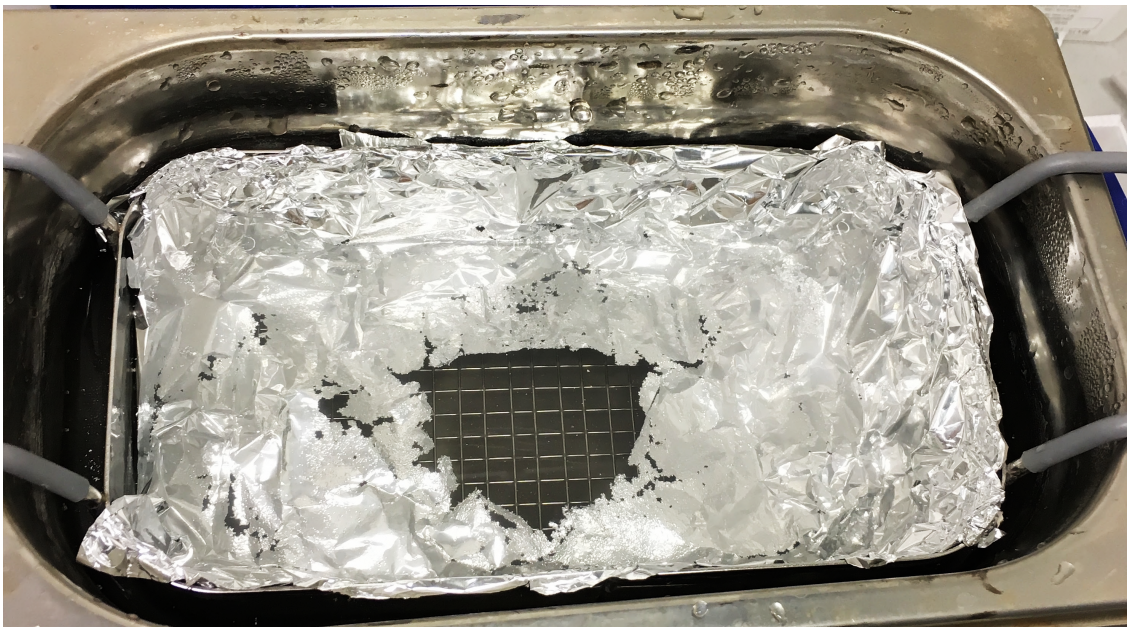

Figure 13: Alumium foil test performed in a bath sonicator in order to determine the hot spot in the bath, which is where the foil is mostly perforated.

Due to variable hot spots in the bath, results obtained by this method are not fully reproducible. In addition, the small filling volume tank limits the possibility of upscale. However, the bath sonication method was adequate for trying out different solvents, regardless of their toxicity, since the vials could be closed during sonication.

On the other hand, the probe-type sonication method is more reproducible, even though this can vary slightly depending of the depth of the probe in the sample, which cannot always be exactly the same. Another advantage of this method compared to the bath sonication is the chance to upscale, made possible by increasing the amount of the sample and the amplitude of the sonication power, meaning by increasing the energy input into the sample.

The hydrodynamic radii of BNNSs prepared with bath sonication (approximately 100 nm) are smaller than the radii of those prepared with probe-type sonication (about 150-200 nm). Since the hydrodynamic radius only refers to how a particle diffuses within a solvent, the lateral radius of a disc-like particle calculated using the thickness obtained from SAXS, is not the same as the hydrodynamic one; it is larger.

In the case of bath sonication, the lateral radius of the nanosheets, which was calculated for sheets with a thickness of 4 nm, since most particles have an approximate thickness of 4 nm, determined by SAXS, is approximately 150-200 nm. The calculated lateral radius of BNNSs exfoliated *via* probe-type sonication is about 250-300 nm. This was estimated for a thickness of 10 nm.

The direct comparison of the lateral radii from both methods is shown in figure 14.

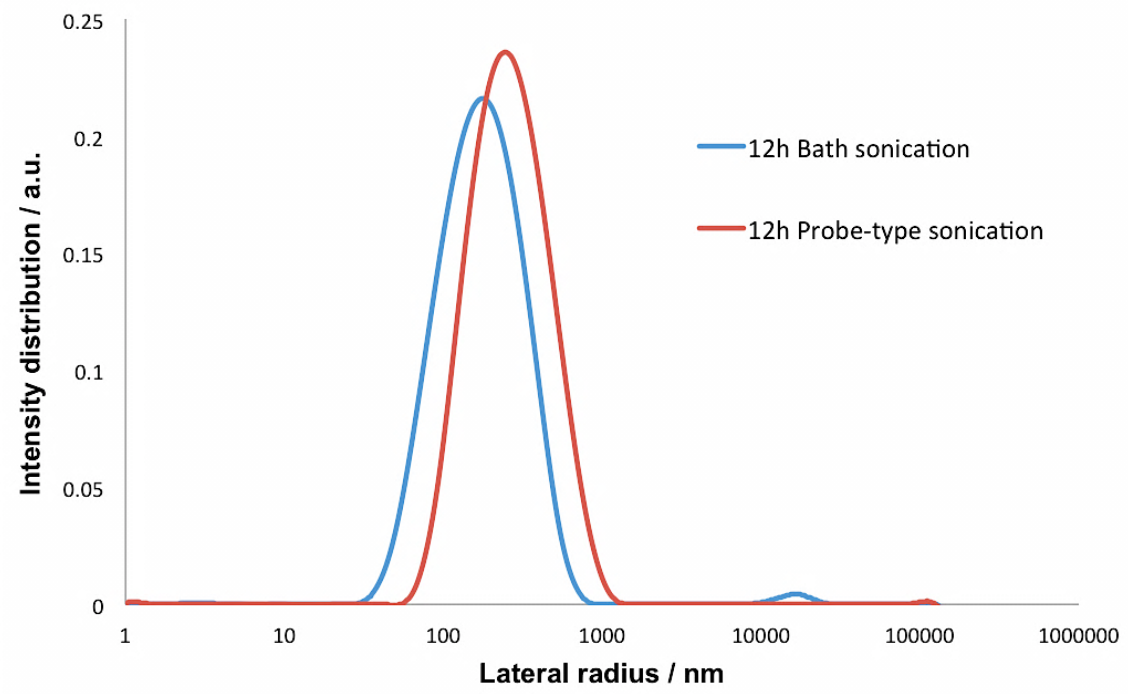

Figure 14: Comparison of the lateral radii of BNNSs from both sonication methods. Bath sonication: 150-200 nm; probe-type sonication: 250-300 nm.

The BNNSs exfoliated *via* probe-type sonication have a bigger lateral radius, as well as a higher scattering intensity, which is a result of the bigger radii.

The size and shape of the particles were investigated by SAXS.

To gain information about the shape, the slope of the scattering curve was evaluated in the so-called Guinier regime. For disc-like particles, the slope is -2.

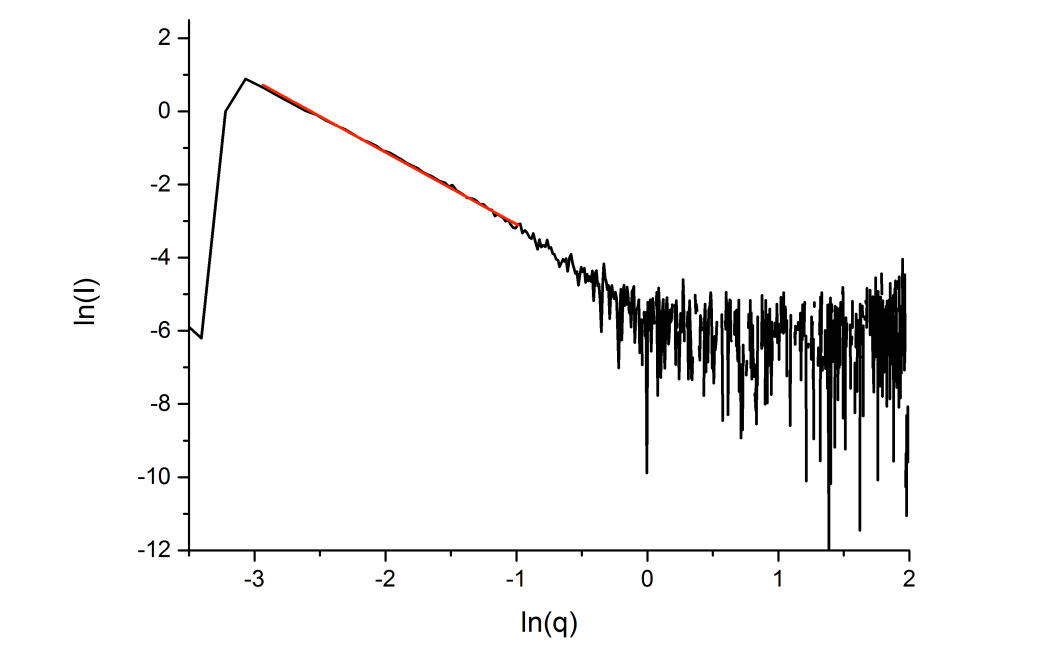

Figure 15: Linear fit of the scattering curves in the Guinier regime for nanosheets prepared by bath sonication method; the value of the slope is - 1.97 ± 0.01.

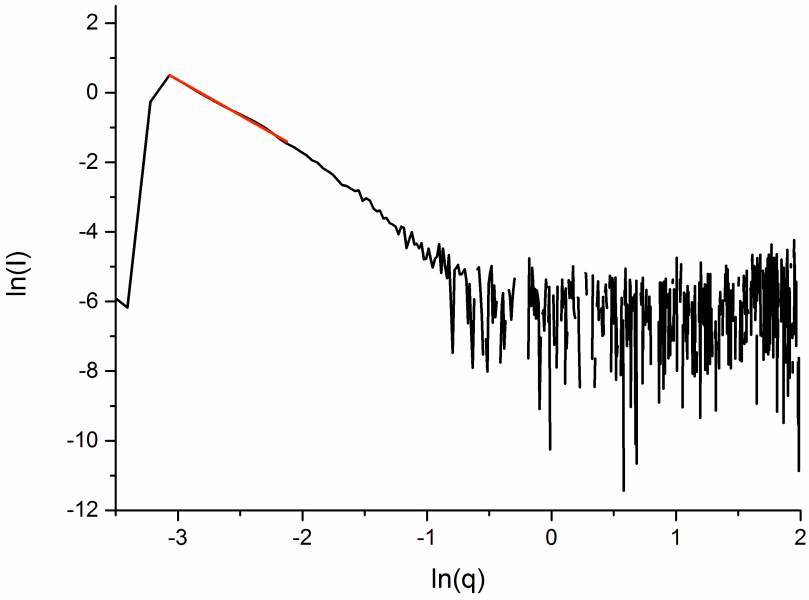

Figure 16: Linear fit of the scattering curves in the Guinier regime for nanosheets prepared by probe-type sonication method; the value of the slope is - 2.03 ± 0.03.

The plate-like shape of BNNSs exfoliated *via* bath sonication and probe-type sonication was confirmed by the value of the slope being approximately - 2.

The pair distance distribution functions of the thickness of the samples in the case of bath sonication do not differ much from each other. (Fig. 17) The average thickness of the exfoliated nanosheets is approximately 4-6 nm, but there are also sheets at a thickness of up to 20-22 nm. In the case of probe-type sonication, a slightly difference between the $p_t(r)$ functions can be observed. (Fig. 18) The BNNSs exfoliated after 2 hours of sonication are thinner, approximately 6-7 nm, in comparison to the sheets that are exfoliated later, which have an average thickness of about 12-15 nm. A reason for that could be that in the beginning of the sonication process, sheets that are on the surface of the bulk crystal containing only a few layers of BN are easier to peal off than the layers that are deeper in the bulk, which get exfoliated later in the sonication process. Another reason might be the aggregation of the sheets after a few hours of sonication, due to the high temperatures that are reached in the solvent, because of the high sonication energy, or because of the saturation of the solvent, as explained in the upcoming section "Recycling". The overall average of the sheet thickness of BNNSs, obtained with the probe-type sonication is about 10-12 nm.

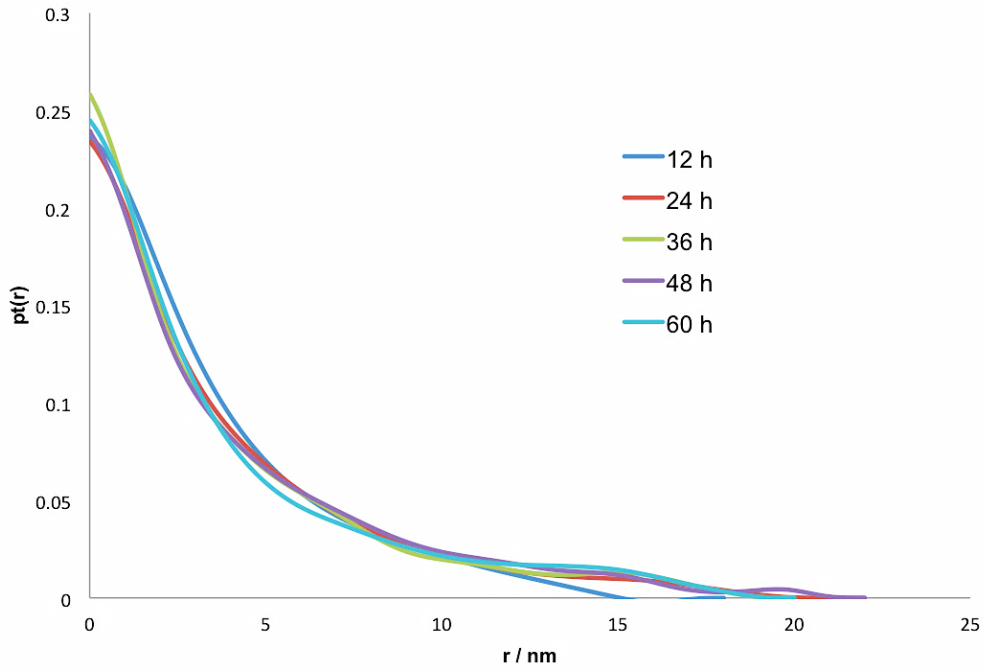

Figure 17: Pair distance distribution functions of thickness of the sample sonicated with ultrasonic bath. The average thickness of the nanosheets is about 4-6 nm.

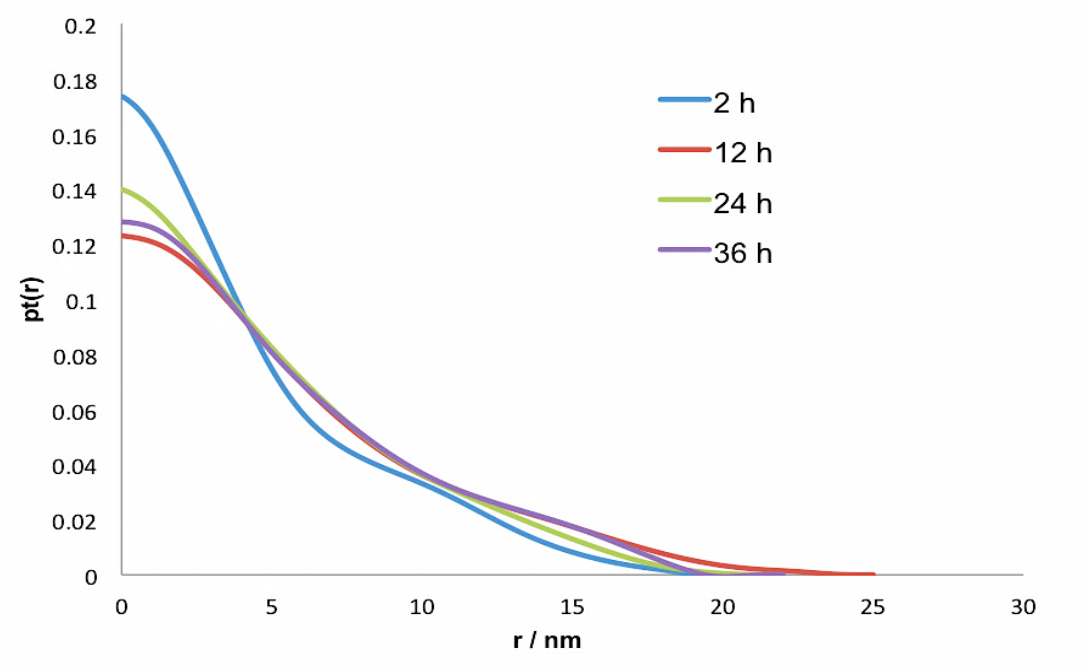

Figure 18: Pair distance distribution functions of thickness of the sample sonicated with probe-type sonicator. The average thickness of the nanosheets is about 10-12 nm.

In conclusion, the liquid phase exfoliation in isopropanol using both the probe-type and the bath sonication method produces thin, disc-like, two dimensional boron nitride nanosheets. The sizes of the sheets prepared with both methods are summarized in the table below.

Method	Lateral radius / nm	Sheet thickness / nm
Bath sonication	150-200	4-6
Probe-type sonication	250-300	10-12

Table 3: Sizes of the BNNSs achieved with probe-type sonication (250-300 nm lateral radius and 10-12 nm thickness) and bath sonication (150-200 nm lateral radius and 4-6 nm thickness).

BNNSs prepared by bath sonication have a lateral radius of about 150-200 nm and a thickness of approximately 4-6 nm, whereas the nanosheets prepared by probe-type sonication are around 10-12 nm thick and have an average lateral radius of about 250-300 nm.

Even though the BNNSs obtained by bath sonication are smaller in diameter and thinner than those obtained by probe-type sonication, the probe-type sonication method was chosen for further experiments, because of the higher yields achieved, as demonstrated below. (Fig. 19)

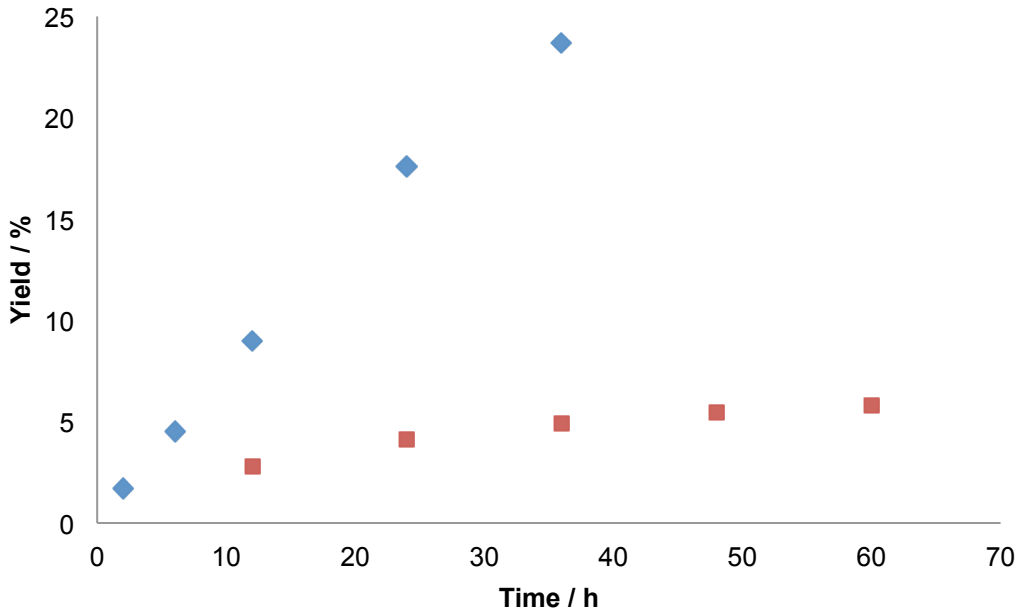

Figure 19: Yields achieved by probe-type (max. 23.71 %) and bath sonication (max. 5.81 %). Probe-type, separated every 2h (blue); Bath, separated every 12h (red).

A faster and more abrupt increase of the yield was observed in the case of probe-type sonication, making this a more favorable technique on producing nanosheets in high amounts. In addition, increasing the amplitude of the probe, meaning the energy input, as well as the volume of the sample, increases the amount of the exfoliated nanosheets, which offers the possibility of upscale.

In order to gain a deeper insight on how the boron nitride nanosheets look like, TEM pictures were made. (Fig. 20-22)

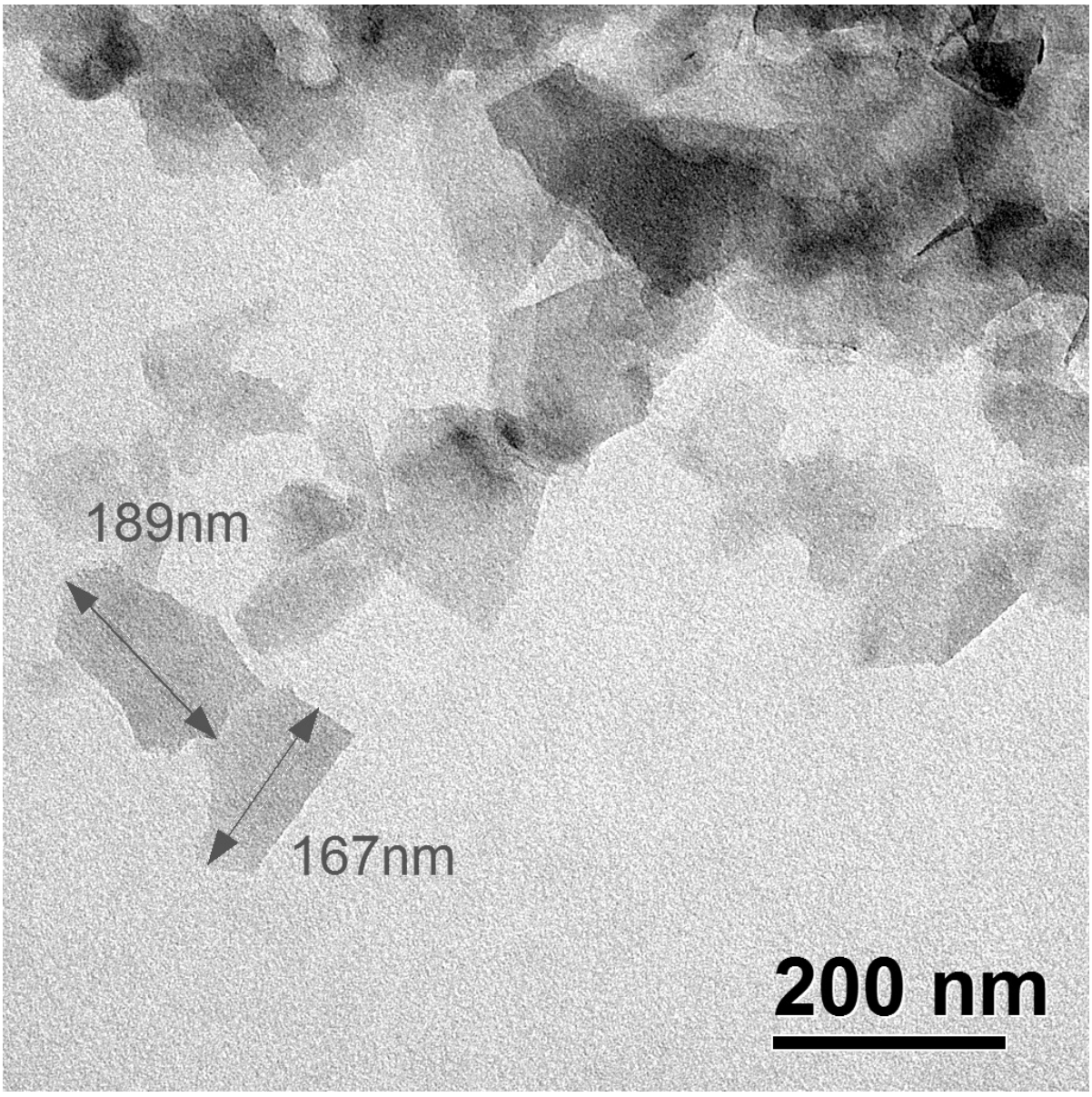

Figure 20: TEM picture of exfoliated BNNSs.

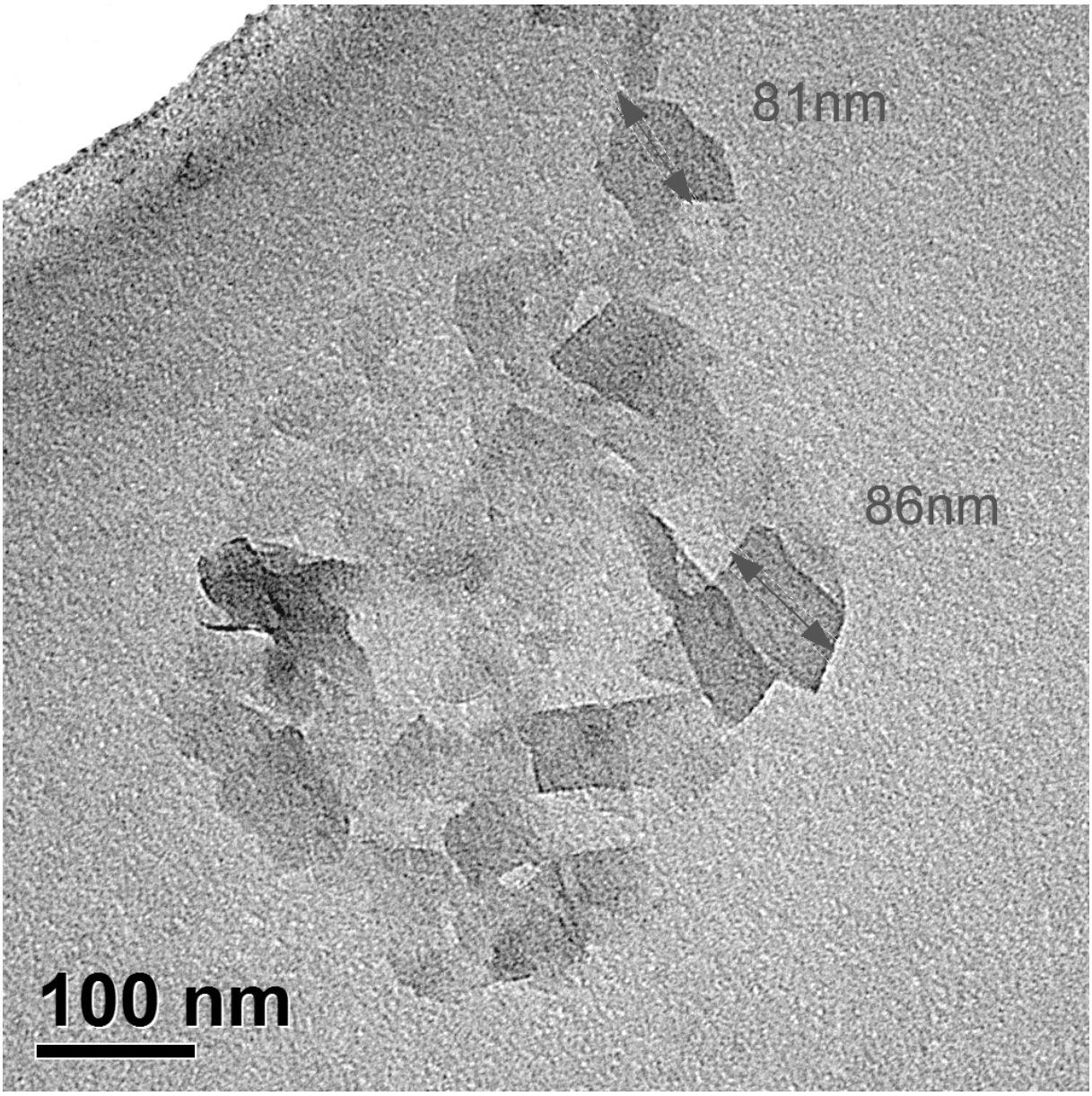

Figure 21: TEM picture of exfoliated BNNSs.

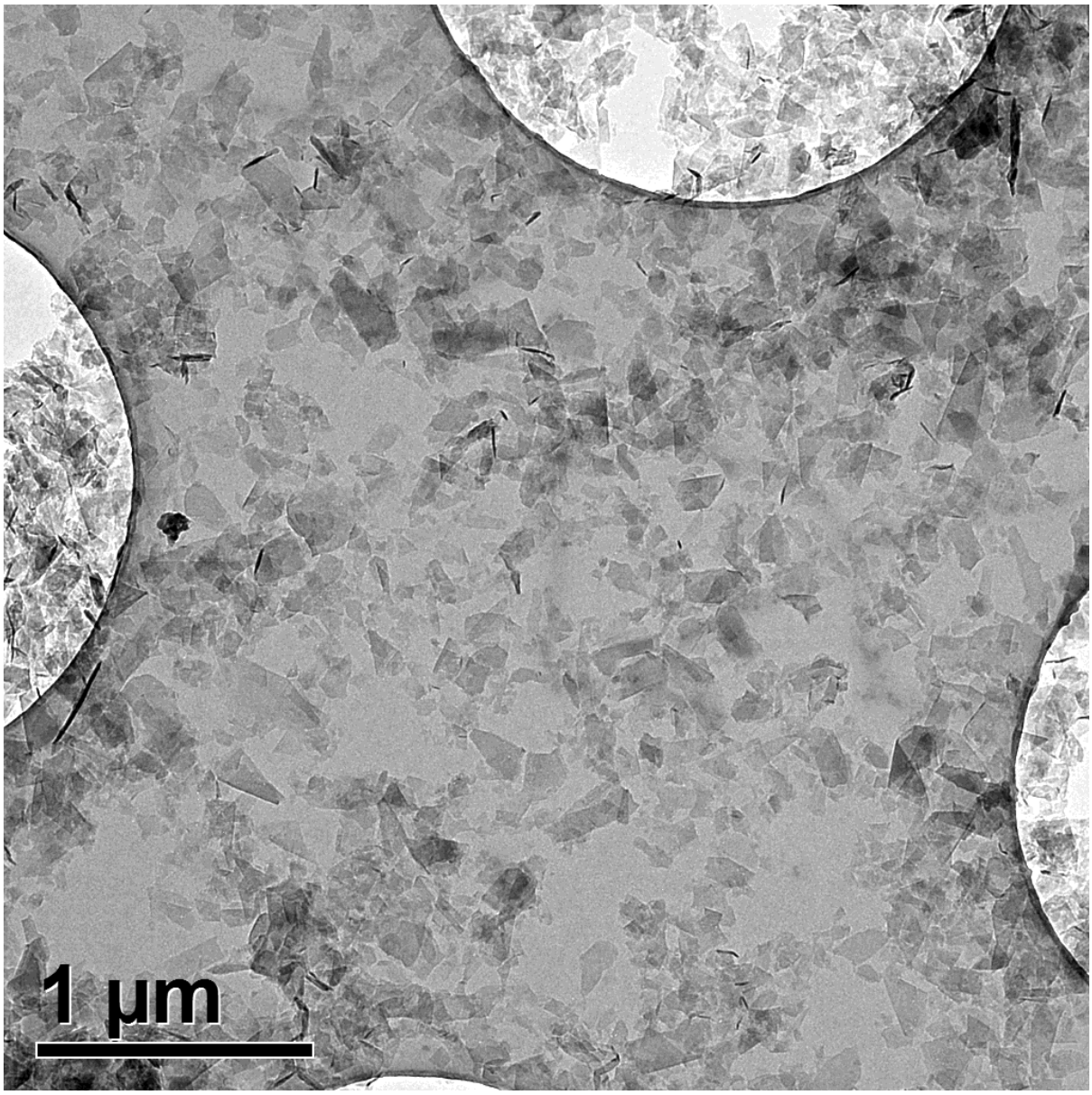

Figure 22: TEM picture of exfoliated BNNSs.

The TEM pictures show that there is a mixture of different lateral radii and thickness of BNNSs. However the highest distribution of the radii is around 100-200 nm. The contrast between a nanosheet and the background represents the thickness of the sheet, meaning the bigger the contrast, the thicker the BNNS. The different contrasts indicate different thicknesses of the exfoliated nanosheets, ranging from monolayers to a few layered sheets.

Some boron nitride nanoscrolls were also observed, shown as small black lines in the picture. The reason why some of the nanosheets are rolled up in tubes, whereas others, or rather the majority of them, remain in their two dimensional form, can not be explained yet. It could be that, a very thin sheet, or some particular lateral diameter to thickness ratio leads to the creation of nanoscrolls, or maybe the reason might be some other external stimulus. However, BNNSs with different thicknesses and lateral radii are produced. The preparation of a homogenous dispersion containing only nanosheets of a certain diameter and thickness is hard to achieve, since there is not a way yet to separate these sheets from other forms of nanoparticles such as nanotubes or nanosheets of other parameters.

The probe-type sonication shows the highest efficiency, but with this method, only one sample at a time can be prepared, whereas with the bath sonication method, it is possible to sonicate a few samples at the same time. The bath sonication method also allows for the vials to be closed during sonication, preventing any contamination of the sample. Closed vials are also optimal for experiments in toxic solvents like acetonitrile or N-methyl-2-pyrrolidone. However, since only isopropanol is being used as an exfoliation solvent and the aim of this work is the production of boron nitride nanosheets in high yields and the production upscale, the probe-type sonication method is more suited.

2.3. Recycling

The yield of BNNSs could be increased up to 23 % by recycling the non-exfoliated boron nitride *via* probe-type sonication. In order to gain as much BNNSs as possible, the exfoliated nanosheets were separated from the bulk crystal by centrifugation and sonicated again in fresh solvent. The resulted yields are shown in figure 23.

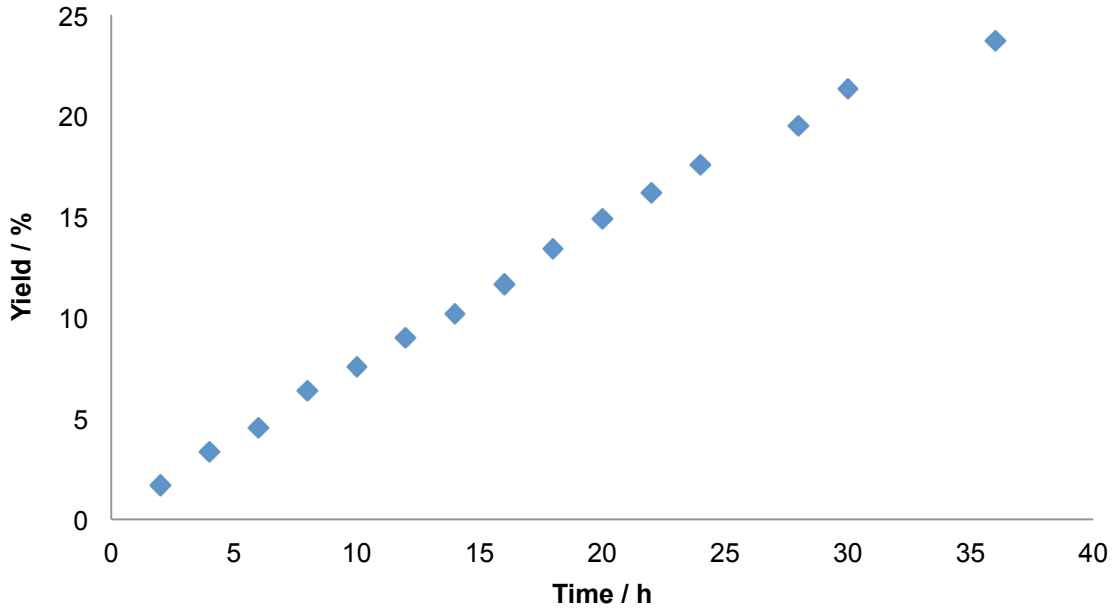

Figure 23: Yield in total (23.71 %); nanosheets prepared by probe-type sonication, recycled every two hours; BNNSs separated by centrifugation.

After 36 hours sonication time in total, a yield of 23.7 %, which corresponds to about 23.7 mg of BNNSs was achieved. This is higher than the yields that are known in the literature. [4-7]

Even though it seems impossible for now to fully exfoliate the boron nitride, obtaining around 23 mg of nanosheets out of 100 mg bulk crystals is a very promising result, as well as the fact that the non-exfoliated boron nitride is not a waste but can be recycled. The yield, at an average of around 1.5 %, is almost constant in each recycling step. However, the final concentration of the nanosheets is low.

The high yield achieved with the probe-type sonication method, when separating the BNNSs every 2 hours, in comparison with sonicating the sample for 12 hours straight without separating the exfoliated nanosheets (Fig. 24) indicates that a kind of an equilibrium between the exfoliated sheets and the bulk crystal is formed, or that a saturation of the solvent is reached.

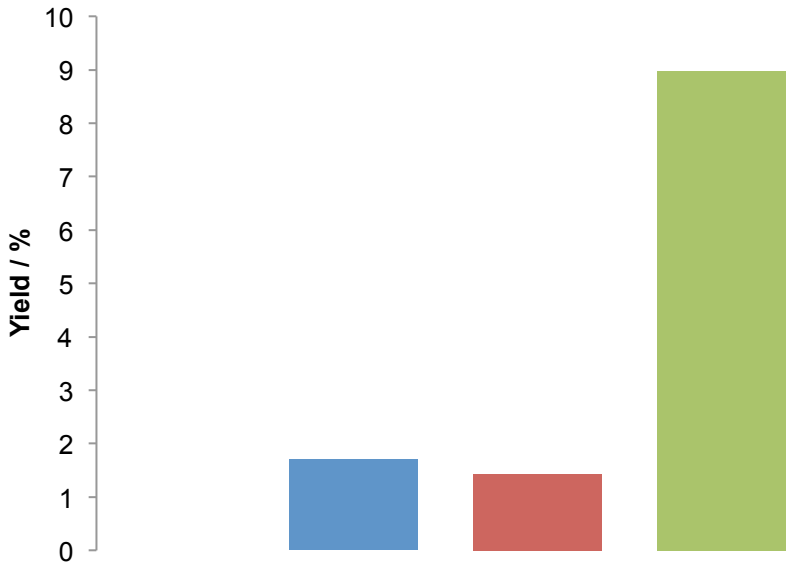

Figure 24: Comparison of the yield achieved by probe-type sonication method; 2h sonication (blue), 12h sonication without separation (red), 12h sonication with separation every 2 hours (green).

After the boron nitride nanosheets are exfoliated, they should be separated from the bulk crystal to avoid re-aggregation of the sheets to the bulk. This phenomenon is also called Ostwald ripening, which says that large particles, which are more energetically favored than smaller particles, grow at the expanse of the smaller ones.

With this in mind, and the fact that after sonicating the sample for a while, there is an equilibrium formed between the nanosheets and the bulk, sonication for longer hours is of no use. Besides, the shorter the sonication process, the less energy it is used and the smaller the probability of contamination. An ideal length of sonication must be specified, since no new nanosheets can be exfoliated after equilibrium is set. How long the sample should be sonicated depends on the initial concentration of boron nitride, the volume, type of vessel and the energy input.

2.4. Upscaling

In order to commercialize the boron nitride nanosheets and be able to use them for different applications, a bigger amount of these sheets, bigger than just a few milligrams, is required. A yield of 23 % looks promising, but the corresponding 23 mg of BNNSs, obtained from the initial 100 mg hexagonal boron nitride, are not enough for applications, so an upscale of the method is of great importance. Increasing the initial concentration resulted in lower yields, but higher amounts of BNNSs, as shown below. (Fig. 25, 26)

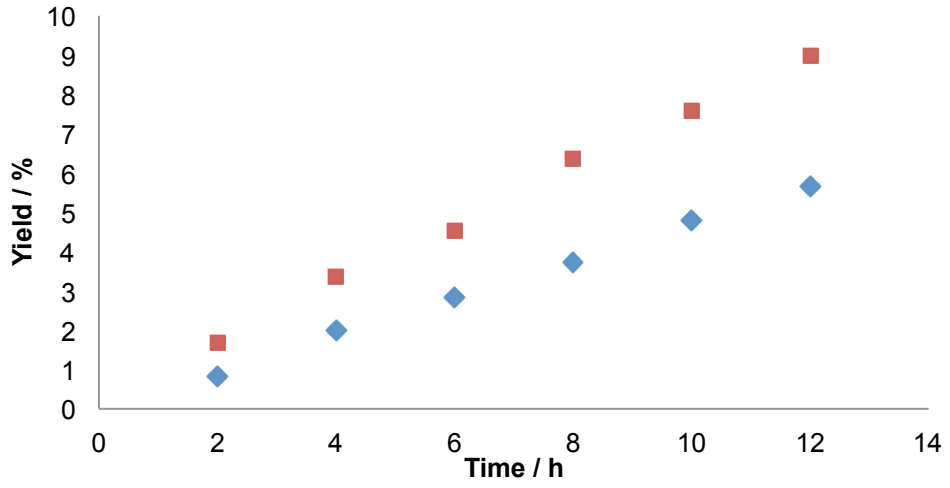

Figure 25: Comparison of the yield when using different initial concentrations; c_i=100 mg/ml (blue), c_i=10 mg/ml (red).

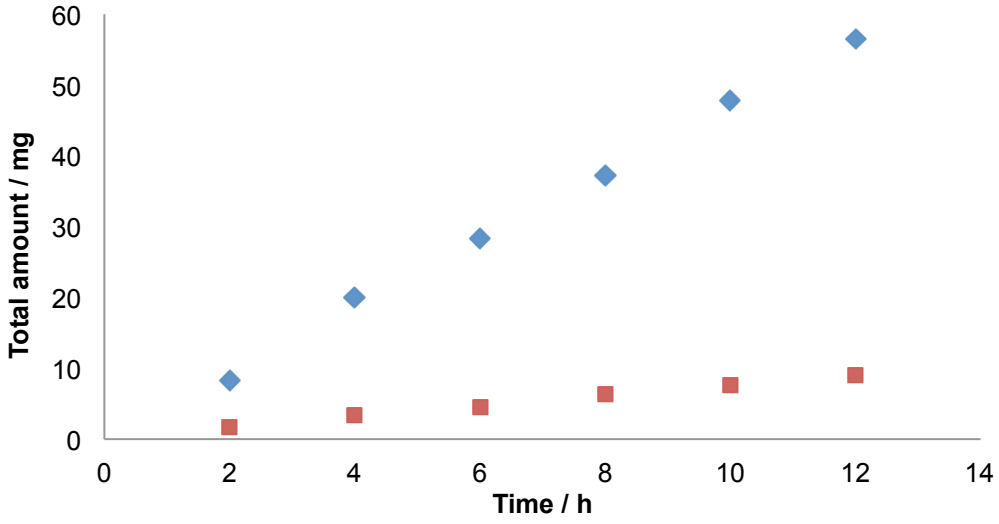

Figure 26: Comparison of the BNNSs amount when using different initial concentration; c_i=100 mg/ml (blue), c_i=10 mg/ml (red).

So, in order to achieve as much exfoliated boron nitride nanosheets as possible, the decision was made to continue the improvement of the probe-type sonication method with an initial concentration of hexagonal boron nitride of 100 mg/ml. Going from an initial concentration of 10 mg/ml in 10 ml solvent, to 100 mg/ml in 100 ml solvent, means also putting more energy into the sample. So the amplitude was increased to 70 %. The dispersion was given in a beaker glass. It is important for the sonicator tip to be well dipped into the dispersion, for an ideal distribution of the energy in the sample. (Fig. 27)

Figure 27: The sonicator probe and the boron nitride dispersion in a beaker glass. The sonicator tip should be well dipped into dispersion for an ideal distribution of the energy in the sample.

The sample was sonicated for 11 hours. A small sample was taken every hour to follow the production of the BNNSs. (Fig. 28)

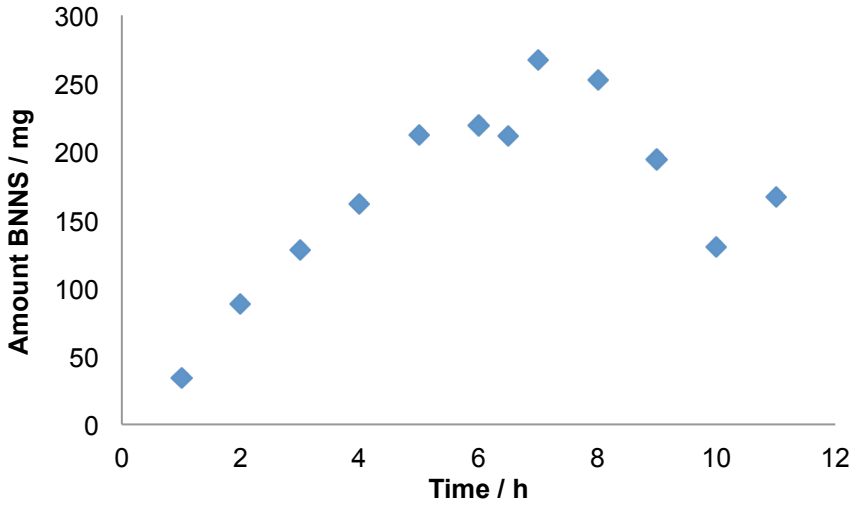

Figure 28: Tracking of the produced amount of BNNSs by probe-type sonication in a beaker glass at an amplitude of 70 %; c_i=100 mg/ml.

The highest amount of exfoliated nanosheets is achieved after seven hours of sonication, meaning it is not necessary to sonicate longer than that.

The BNNSs were acquired by 10 minutes centrifugation at 2500 rpm. Since the hydrodynamic radius is the same (Fig. 29), the lower speed was chosen, because it leads to higher amounts of BNNSs.

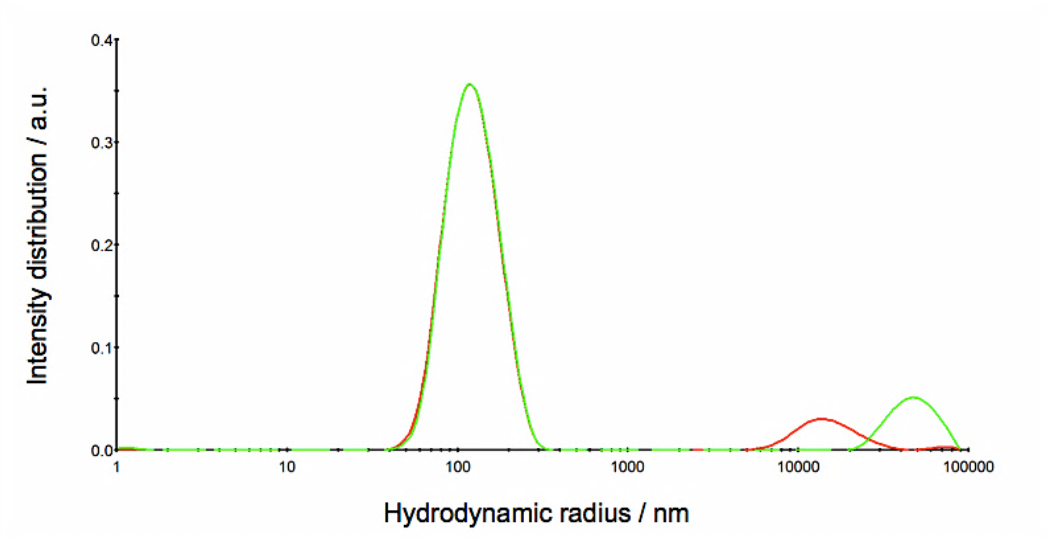

Figure 29: Comparison of the hydrodynamic radii of the nanosheets acquired by centrifugation at a speed of 2500 rpm (green) and 4500 rpm (red).

DLS shows that the average hydrodynamic radius of the BNNSs is about 80-100 nm.

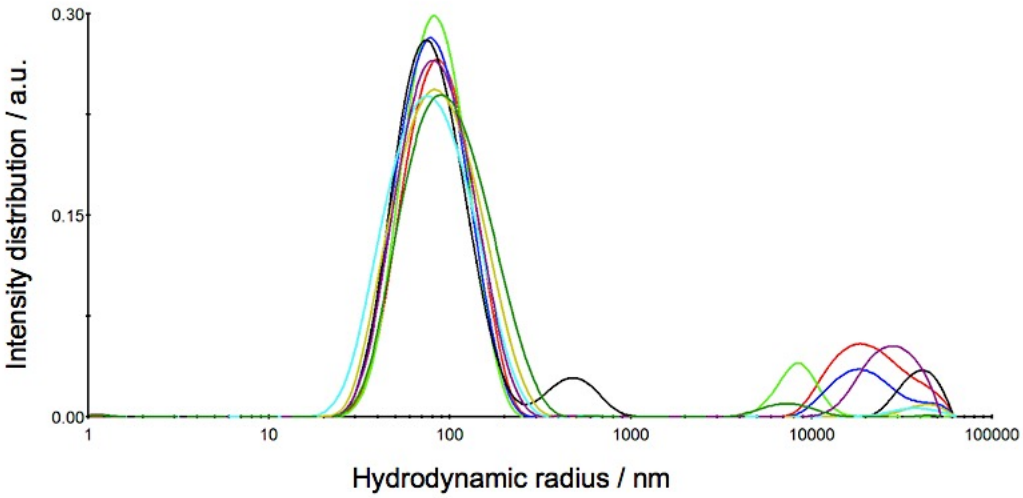

Figure 30: Hydrodynamic radii of BNNSs from 1 to 8 hours of probe-type sonication at 70 % amplitude; 2 ml sample was taken every hour in order to follow the exfoliation process.

Even though separating the sample every two hours, or in the previous case every seven hours works, this would not be a practical solution in the long run, since it costs a lot of time, energy and work. For example the time needed for the preparation of about 1 g of BNNSs would be around 270 hours, which corresponds to about 34 work days and approximately 7 weeks.

In order to reduce the time needed for the exfoliation, the idea was to dilute the sample after a few hours of sonication and stir it. Due to sonication process, the layers get loosened and there is enough solvent for the BNNSs to be dispersed in before the equilibrium is reached. Stirring the sample without a previous sonication treatment does not exfoliate the nanosheets. So after total 11 h sonication, when the saturation of the solvent is reached and no new BNNSs are exfoliated, the sample was diluted and stirred for one hour. (Fig. 31)

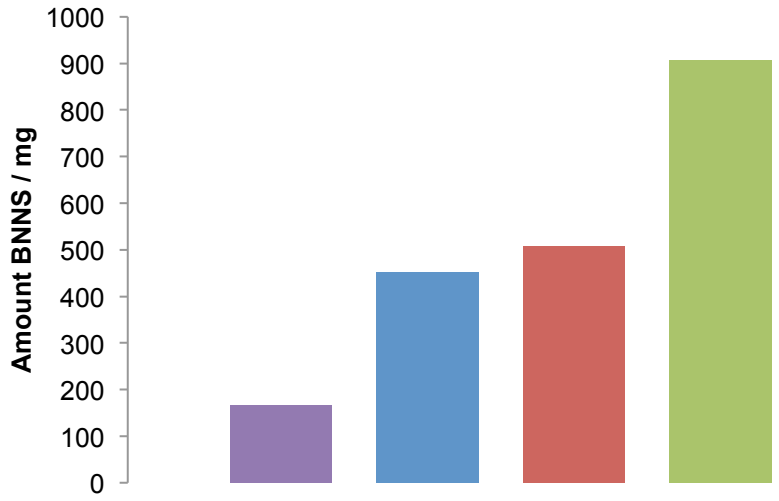

Figure 31: Different dilution ratios; 11 h probe-type sonication at 70 % amplitude (purple); after dilution the sample was stirred for 1h: 1:10 (blue), 1:100 (red), 1:1000 (green).

The most promising dilution ration would be the 1: 1000 ration, which would produce about 900 mg BNNSs. However, this would mean that in the end of the liquid phase exfoliation process, these 900 mg BNNSs would be dispersed in 100 L solvent. Since, there is no way yet how to reduce the volume of the solvent while preventing the aggregation of the nanosheets during the process, this dilution ratio isn't very favorable at the moment. The dilution ratio 1:100 could be a manageable choice though. The method is demonstrated in figure 32.

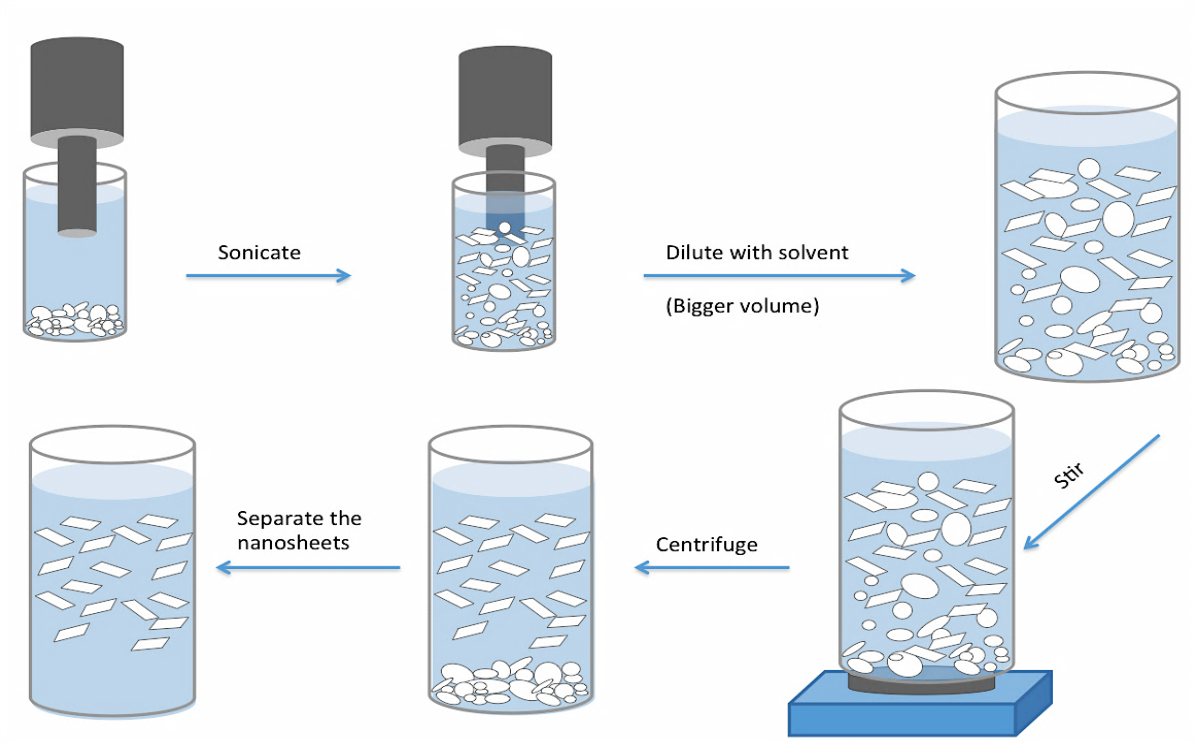

Figure 32: Improved liquid phase exfoliation; after sonication, the sample is diluted and stirred; the BNNSs are separated by centrifugation.

In conclusion, starting with a concentration of 100 mg/ml *h*-BN in 100 ml isopropanol in a beaker glass and sonicating the sample for about six to seven hours with a probe-type sonicator at an amplitude of 70 %, and afterwards diluting and stirring the sample for one or two hours shows very promising results.

So combining these results with the fact that with every recycling step, almost the same amount of boron nitride nanosheets is produced, can lead to the production of higher amounts of nanosheets in shorter amount of time.

However, the final concentration of BNNSs is too low, so reducing the volume of the solvent is the next necessary step to take. The removal of the solvent is also crucial, because the BNNSs should be solvent-free for their integration in a polymer matrix.

2.5. Reducing / exchanging the solvent

The BNNSs were dried by fully removing the solvent *via* rotary evaporation. However, this led to aggregation of the sheets to bigger bulk crystals and reversing the aggregation by re-dispersing in fresh solvent and agitating was not possible. The rotary evaporation was then used to only reduce the solvent, not remove it all; this also led to irreversible aggregation of the nanosheets. Other methods, such as evaporation of the solvent through stirring while the vial was open, evaporation through standing open in the air, and filtration were performed, but unfortunately these were not very successful either. All these methods lead to coagulation of the particles, which is the irreversible collapse of the colloid into a bulk phase. Re-dispersion is not possible anymore, without a high-energy input. However, when a vial containing BNNSs in isopropanol was sonicated in the ultrasonic bath for 2.5 hours, while being open for the solvent to evaporate, DLS showed that the hydrodynamic radius did not increase much. (Fig. 33)

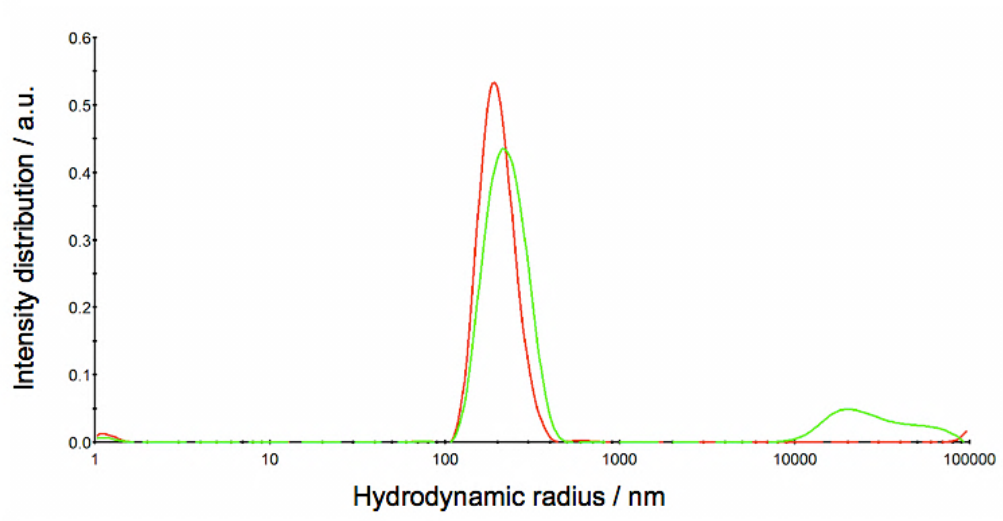

Figure 33: Hydrodynamic radius of BNNSs before (red) and after evaporation of the solvent for 2.5 h in ultrasonic bath (green).

This method still needs further investigation with respect to bigger volumes.

Since isopropanol is not favored for the epoxy resin for which these boron nitride nanosheets are prepared, because it initiates polymerization, it is important to eliminate or exchange the solvent. Long high-speed centrifugation, was performed.

A schema of this process is demonstrated in figure 34.

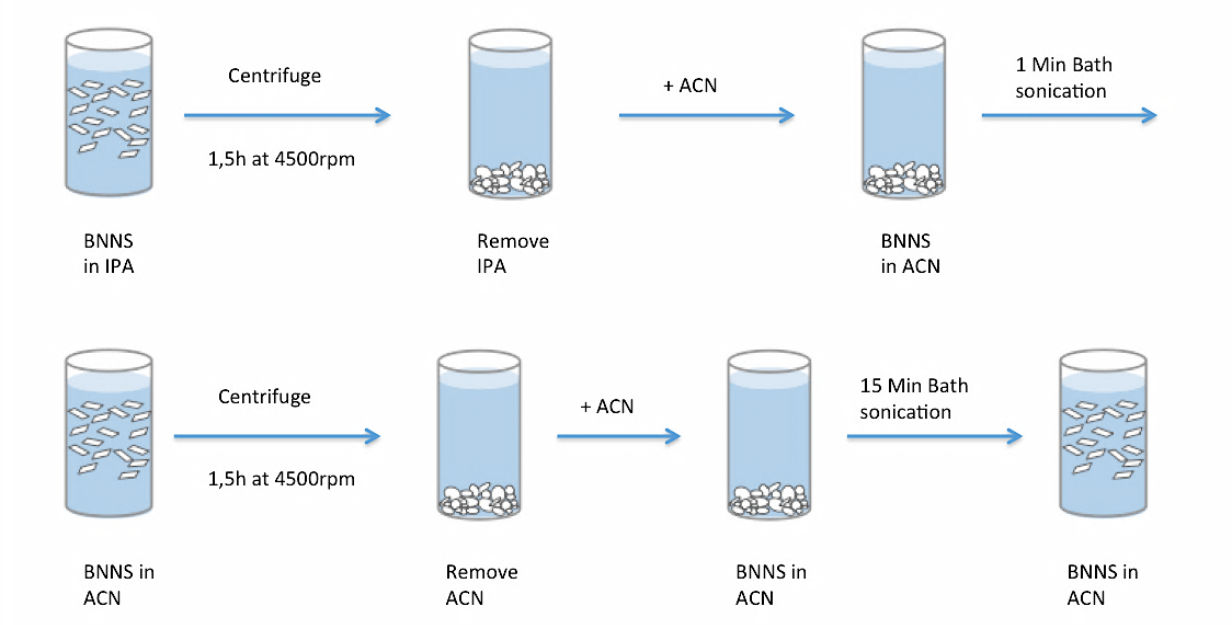

Figure 34: Long high-speed centrifugation (1.5 h at 4500 rpm) to exchange the solvent from isopropanol to acetonitrile.

The sample was centrifuged for 1.5 hours at a speed of 4500 rpm. Then the solvent, in this case isopropanol was removed and acetonitrile was added to the sediment. The sample was sonicated for one minute in ultrasonic bath, in order to re-disperse the BNNSs in acetonitrile. Then the sample was centrifuged again for another 1.5 hours at 4500 rpm. The acetonitrile was removed, fresh acetonitrile was added and the sample was sonicated for 15 minutes in ultrasonic bath, so that the nanosheets could be re-dispersed well in the solvent. In the end of the process the BNNSs were dispersed in the new solvent, acetonitrile. UV-Vis, DLS and SAXS were performed to characterize the amount, size and thickness of the BNNSs after the process of the long high-speed centrifugation.

Sample	Yield / %	Amount BNNSs / mg
6 h sonication	1.14	2.3
IPA after 1.5 h at 4500 rpm	0.10	0.2
ACN after 1.5 h at 4500 rpm	0.07	0.1
BNNSs in ACN	1.11	2.2

Table 4: Yield and amount of BNNSs before and after long high-speed centrifugation.

The amount of BNNSs after the long high-speed centrifugation doesn't change much, indicating that there is a negligible loss of nanosheets during the process. The similar hydrodynamic radii (Fig. 35) also illustrate that no aggregation occurred during the centrifugation.

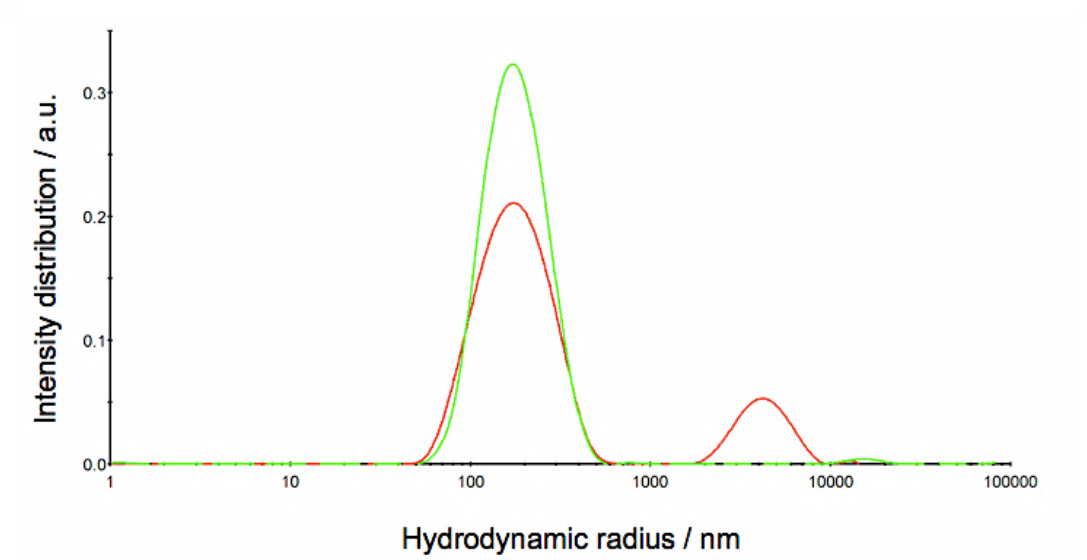

Figure 35: Hydrodynamic radii of BNNSs before (red) and after long high-speed centrifugation (green).

However, SAXS shows that the nanosheets get thicker. Before the process they had a thickness of about 10 to 12 nm (Tab. 3) and afterwards they can be up to 25 nm thick. (Fig. 36)

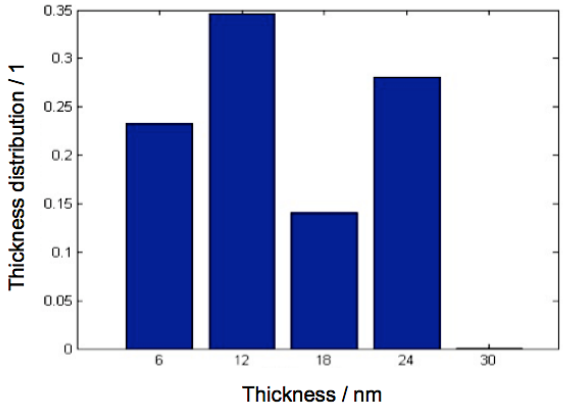

Figure 36: Thickness distribution of BNNSs after long high-speed centrifugation.

Yet, this process is more promising than the other ones performed for the reduction of the solvent. Even so, these methods still need further investigation for upscale.

CONCLUSION AND OUTLOOK

In conclusion, the liquid phase exfoliation was optimized in order to fabricate high amounts of boron nitride nanosheets, for their application as filler compound in polymers and polymer-based composites to improve their thermal conductivity.

Isopropanol was proven to be the better solvent for the exfoliation and the probe-type sonication was chosen as a more suitable method to achieve a high amount on BNNSs. The probe-type sonication method is more reproducible compared to the bath sonication and it offers the chance to upscale, which is made possible by increasing the amount of the sample and the amplitude of the sonication power, meaning by increasing the energy input into the sample.

An initial concentration of layered boron nitride of 100 mg/ml, dispersed in 100 ml isopropanol showed the most promising results. After 7 hours of sonication at an amplitude of 70 %, about 270 mg of BNNSs were obtained. Diluting the sample with a dilution ratio of 1:100 and stirring it for one to two hours results in the exfoliation of approximately 500 mg nanosheets. Since recycling the sample leads to the production of similar amounts of BNNSs with each recycling step, about 270 mg exfoliated nanosheets can be obtained every 7 hours of sonication. Combining these results makes it possible to prepare about 1 g of BNNSs in just a few days.

However, the final concentration of the BNNSs still remains low, since in the end of this process, the 1 g of nanosheets will be dispersed in about 1.2 L isopropanol. Hence, reducing, removing or exchanging the solvent is an important step. Fully removing the solvent led to irreversible aggregation of the nanosheets. Therefore, a method to only reduce it while the sample is being sonicated in ultrasound bath was performed. Furthermore, in order to change the solvent from isopropanol to acetonitrile, long high-speed centrifugation was executed. Both these methods show promising results, but because they were only performed with small samples, they still need further investigation with respect to bigger volumes.

Since, as mentioned before, this is a rather new field of research, there are still many things that haven't been explored yet, such as different chemical modifications of the BNNSs, graphene or other 2D materials. Moreover, there might even be some properties that have not been investigated and discovered yet. Producing grams, or even kilograms of boron nitride nanosheets and graphene in a very timesaving, cost-effective way, in order to enable the commercialization of these sheets is a worldwide hot research topic at the moment.

One of the most challenging issues with the production of these materials however, is still their very strong tendency to re-aggregate to their bulk form. Preventing this irreversible coagulation of the nanosheets is of great importance and requires immediate investigation.

The high-yield production method presented in this work, shows promising results, indicating that studies about these nanomaterials are moving in the right direction. More detailed research could lead to a breakthrough with regard to two-dimensional nanosheets and revolutionize the technology.

CHAPTER 3

Experimental

3.1. Preparation and materials

Solvent

The liquid phase exfoliation *via* sonication was performed in the following solvents.

Name	Chemical formula	Details (Purity)	Supplier	CAS – Number
Acetone	C_3H_6O	≥ 99.8 % (GC)	Roth	67-64-1
Acetonitrile (ACN)	C_2H_3N	≥ 99.5 % (GC)	Fluka	75-05-8
Isopropanol (IPA)	C_3H_8O	≥ 99.9 % (GC)	Roth	67-63-0
N-methyl-2-pyrrolidone (NMP)	C_5H_9NO	≥ 99.5 % (GC)	Merck	872-50-4
Polyethylenglycol$_{200}$ (PEG_{200})	$C_{2n}H_{4n+2}O_{n+1}$	Average mol wt 200	Sigma-Aldrich	25322-68-3

Table 5: Different solvents, that were used for the exfoliation.

Vessels used for sonication

The following vessels (4 ml vial for bath sonication, 20 ml vial, glass bottle, beaker glass for probe-type sonication) were used:

Figure 37: Vessels that were used for the liquid phase exfoliation. From left to right: 4 ml vial, 20 ml vial, 50 ml glass bottle, 100 ml glass bottle, 250 ml beaker glass.

Method

Both sonication methods, the bath and the probe-type sonication were used to exfoliate the hexagonal boron nitride to 2D nanosheets. The sample was cooled down during the process; in the case of bath sonication, a cooling coil was used to cool the water in the ultrasound bath, and in the case of probe-type sonication, the vessel was dipped into an ice-bath.

Bath sonication

The ultrasonic bath that was used was Elmasonic S 30. (Fig. 38)

Technical data:

Mains voltage: 115-120 V
Mains frequency: 50 Hz
Ultrasonic frequency: 37 kHz
Ultrasonic power effective: 80 W
Max. filling volume tank: 2.75 L

Figure 38: Ultrasonic bath: Elmasonic S 30.

40 mg *h*-BN bulk crystals were dispersed in 4 ml isopropanol in a 4 ml vial and sonicated in the ultrasonic bath. After 12 hours the BNNSs were separated by 10 minutes centrifugation at 4500 rpm and the remaining boron nitride was dispersed in 4 ml fresh isopropanol and sonicated for another 12 h. The process was repeated up to 60 hours total.

Probe-type sonication and recycling

The probe-type sonicator that was used was Sonics & Materials, 400 Watt- Model. (Fig. 39)

Technical data:

Variable power:	max. 400 W
Frequency:	20 kHz
Probe:	standard horn ½" (13mm) with threaded end and replaceable tip
	replaceable tip ½" (13mm)
Probe material:	titanium alloy (Ti-6Al-4V)

The samples were sonicated with an On/Off puls of 0.5/0.5 seconds.

Figure 39: Probe-type sonicator, Sonics & Materials, 400 Watt- Model.

100 mg *h*-BN bulk crystals were dispersed in 10 ml isopropanol in a 20 ml vial and sonicated at an amplitude of 30 %. The sample was cooled with ice bath. After 2 hours of sonication, the exfoliated BNNSs were separated by 10 a minute centrifugation at 4500 rpm. The remaining non-exfoliated boron nitride was re-

dispersed in fresh 10 ml isopropanol and sonicated for another 2 hours. This process was repeated several times, up to a total of 36 hours.

Upscaling

1 g *h*-BN bulk crystals were dispersed in 10 ml isopropanol in a 20 ml vial and sonicated at an amplitude of 30 %. After 2 hours of sonication, the exfoliated BNNSs were separated by 10 a minute centrifugation at 4500 rpm. The remaining non-exfoliated boron nitride was re-dispersed in fresh 10 ml isopropanol and sonicated for another 2 hours. This process was repeated several times, up to a total of 12 hours. The sample was cooled with ice bath.

10 g *h*-BN bulk crystals were dispersed in 100 ml isopropanol in a beaker glass and sonicated at an amplitude of 70 %.

3.2. Characterization

Ultraviolet – visible spectroscopy (UV –Vis)

The concentration of the exfoliated BNNSs was measured by UV-Vis spectroscopy, by using the Lambert – Beer law:

$$A = \log_{10} (I_0/I) = \varepsilon\, c\, d \qquad (1)$$

The absorption of boron nitride nanosheets is in the ultraviolet range and the extinction coefficient at a wavelength of 300 nm is 2354 L / (g m). [4]

The photometer that was used was the Aligent Cary 60 Spectrophotometer. (Fig. 40)

Electrical specifications:

Main supply:	standard 3.2 A/12 V plug pack
Spectrophotometer:	90-265 V AC
	frequency 47-63 Hz

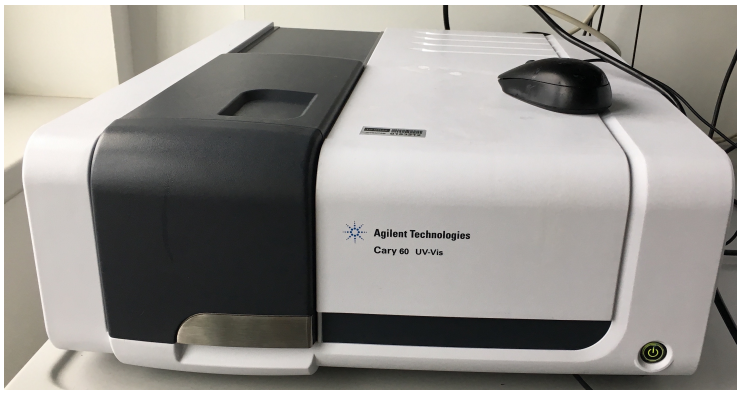

Figure 40: Aligent Cary 60 Spectrophotometer.

Dynamic light scattering (DLS)

DLS was used to determine the hydrodynamic radius of the nanosheets, which is related to the lateral radius, as explained in chapter 1.6. The radius distribution was calculated with ORT (optimized regulation technique) program [132] using inverse Laplace.

The DLS equipment that was used (Fig. 41) comprises a goniometer, a diode laser working at λ=532 nm (Coherent Verdi V5) with single mode fiber detection optics (OZ from GMP, Zürich, Switzerland), an ALV/SO-SIPD/DUAL photomultiplier with pseudo-cross-correlation mode [133], and an ALV 7004/ Digital Multi Tau Real Time Correlator (ALV, Langen, Germany). Correlation functions were averaged with 10 measurements of 30 s. [133]

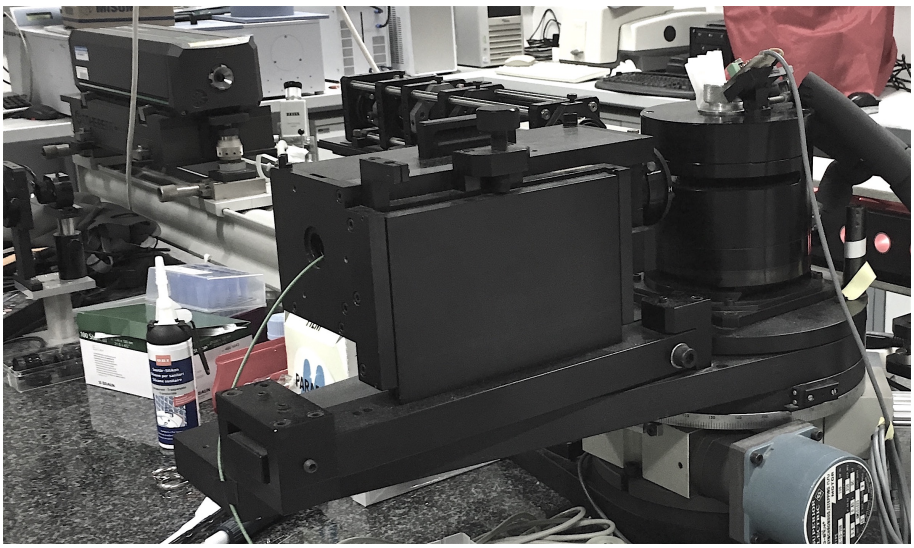

Figure 41: Dynamic light scattering equipment with diode laser working at λ=532 nm.

Small angle X – ray scattering (SAXS)

The thickness of the BNNSs was determined by SAXS. The equipment that was used was the SAXSess from Anton Paar. (Fig. 42) The SAXS equipment consisted of a slit-geometry camera with high flux and low background (SAXSess, Anton Paar, Graz, Austria), connected to an X-Ray generator (DebyeFlex 3000), operating at 40 kV and 50 mA with a sealed tube Cu anode. [133] The Detector that was used was the 1D-Diode array detector: Mythen 1K (Dectris, Switzerland), 1280 pixels a 50 µm. Active length: 6.4 cm. The sample was irradiated 30 times, each time for 60 s.

Figure 42: SAXS equipment; SAXSess from Anton Paar.

Transmission electron microscopy (TEM)

TEM enabled an insight into the shapes and sizes of the BNNSs.

The TEM equipment that was used was the “FEI Tecnai 12” with a maximum accelerating voltage of 120 kV and LaB_6 as an electron source.

TEM magnification:	35 x – 700.000 x
TEM point resolution:	0.34 nm
TEM line resolution:	0.20 nm
Holder:	Single tilt

LIST OF TABLES

LIST OF FIGURES

REFERENCES

[1] M. Auffan, J. Rose, J.-Y. Bottero, G. V. Lowry, J.-P. Jolivet, M. R. Wiesner, *Nat. Nanotechnol.,* **2009**, 4, 634-641.

[2] https://www.nobelprize.org/nobel_prizes/physics/laureates/2010/

[3] W.-L. Song, P. Wang, L. Chao, A. Anderson, M. J. Meziani, A. J. Farr, Y.-P. Sun, *Angew. Chem. Int. Ed.,* **2012**, 51, 6498-6501.

[4] J. Shen, Y. He, J. Wu, C. Gao, K. Keyshar, X. Zhang, Y. Yang, M. Ye, R. Vajtai, J. Lou, P. M. Ajayan, *Nano. Lett.,* **2015**, 15, 5449-5454.

[5] C. Zhi, Y. Bando, C. Tang, H. Kuwahara, D. Golberg, *Adv. Mater.,* **2009**, 21, 2889-2893.

[6] K. L. Marsh, M. Souliman, R. B. Kaner, *Chem. Commun.,* **2014**, 187-190.

[7] Y. Lin, T. V. Williams, T.-B. Xu, W. Cao, H. E. Elsayed-Ali, J. W. Connell, *J. Phys. Chem. C,* **2011**, 115, 2679-2685.

[8] Y. Lin, T.V. Williams, J. W. Connell, *J. Phys. Chem. Lett.,* **2010**, 1, 277-283.

[9] M. Chhowalla, H. S. Shin, G. Eda, L. J. Li, K. Loh, H. Zhang, *Nat. Chem.,* **2013**, 5, 263-275.

[10] X. Huang, Z. Y. Zeng, H. Zhang, *Chem. Soc. Rev.,* **2013**, 42, 1934-1946.

[11] M. S. Xu, T. Liang, M. M. Shi, H. Z. Chen, *Chem. Rev.,* **2013**, 113, 3766-3798.

[12] M. Chhowalla, Z. F. Liu, H. Zhang, *Chem. Soc. Rev.,* **2015**, 44, 2584-2586.

[13] C. Zhi, Y. Bando, C. Tang, H. Kuwahara, D. Golberg, *Adv. Mater.,* **2009**, 21, 2889-2893.

[14] M. Osada, T. Sasaki, *J. Mater. Chem.,* **2009**, 19, 2503-2511.

[15] Q. Wang, D. O'Hare, *Chem. Rev.,* **2012**, 112, 4124-4155.

[16] A. K. Geim, K. S. Novoselov, *Nat. Mater.,* **2007**, 6, 183-191.

[17] K. S. Novoselov, D. Jiang, F. Schedin, T. J. Booth, V. V. Khotkevich, S. V. Morozov, A. K. Geim, *Proc. Natl. Acad. Sci. U.S.A,* **2005**, 102, 10451-10453.

[18] C. R. Dean, A. F. Young, I. Meric, C. Lee, L. Wang, S. Sorgenfrei, K. Watanabe, T. Taniguchi, P. Kim, K. L. Shepard, *Nat. Nanotechnol.,* **2010**, 5, 722-726.

[19] H. Li, J. Wu, X. Huang, G. Lu, J. Yang, X. Lu, Q. H. Xiong, H. Zhang, *ACS Nano,* **2013**, 7, 10344-10353.

[20] V. Nicolosi, M. Chhowala, M. G. Kanatzidis, M. S. Strano, J. N. Coleman, *Science,* **2013**, 340, 1226419.

[21] Y. Hernandez, V. Nicolosi, M. Lotya, F. M. Blighe, Z. Sun, S. De, I. T. McGovern, B. Holland, M. Byrne, Y. K. Gun'Ko, *Nat. Nanotechnol.,* **2008**, 3, 563-568.

[22] J. N. Coleman, M. Lotya, A. O'Neill, S. D. Bergin, P. J. King, U. Khan, K. Young, A. Gaucher, S. De, R. J. Smith, *Science*, **2011**, 331, 568-571.

[23] U. Khan, P. May, A. O'Neill, A. P. Bell, E. Boussac, A. Martin, J. Semple, J. N. Coleman, *Nanoscale*, **2013**, 5, 581-587.

[24] K. R. Paton, E. Varrla, C. Backes, R. J. Smith, U. Khan, A. O'Neill, C. Boland, M. Lotya, O. M. Istrate, P. King, *Nat. Mater.,* **2014**, 13, 624-630.

[25] L. M. Viculis, J. J. Mack, O. M. Mayer, H. T. Hahn, R. B. Kaner, *J. Mater. Chem.,* **2005**, 15, 974-978.

[26] Z. Y. Zeng, Z. Y. Yin, X. Huang, H. Li, Q. Y. He, G. Lu, F. Boey, H. Zhang, *Angew. Chem., Int. Ed.,* **2011**, 50, 11093-11097.

[27] Z. Y. Zeng, T. Sun, J. X. Zhu, X. Huang, Z. Y. Yin, G. Lu, Z. X. Fan, Q. Y. Yan, H. H. Hng, H. Zhang, *Angew. Chem., Int. Ed.,* **2012**, 51, 9052-9056.

[28] K. Parvez, Z.-S. Wu, R. Li, X. Liu, R. Graf, X. Feng, K. Müllen, *J. Am. Chem. Soc.,* **2014**, 136, 6083-6091.

[29] Z. Liu, R. Ma, M. Osada, N. Iyi, Y. Ebina, K. Takada, T. Sasaki, *J. Am. Chem. Soc.,* **2006**, 128, 4872-4880.

[30] J. Liang, R. Ma, N. Iyi, Y. Ebina, K. Takada, T. Sasaki, *Chem. Mater.,* **2010**, 22, 371-378.

[31] Y. Zhang, L. Zhang, C. Zhou, *Acc. Chem. Res.,* **2013**, 46, 2329-2339.

[32] L. Song, L. Ci, H. Lu, P. B. Sorokin, C. Jin, J. Ni, A. G. Kvashnin, D. G. Kvashnin, J. Lou, B. I. Yakobson, *Nano Lett.,* **2010**, 10, 3209-3215.

[33] S. Bae, H. Kim, Y. Lee, X. Xu, J.-S. Park, Y. Zheng, *Nat. Nanotechnol.,* **2010**, 5, 574-578.

[34] M. Choucair, P. Thordarson, J. A. Stride, *Nat. Nanotechnol.,* **2009**, 4, 30-33.

[35] X. Wang, L. Zhi, N. Tsao, Z. Tomovi c, J. Li, K. Mullen, *Angew. Chem., Int. Ed.,* **2008**, 47, 2990-2992.

[36] J. S. Son, J. H. Yu, S. G. Kwon, J. Lee, J. Joo, T. *Adv. Mater.,* **2011**, 23, 3214-3219.

[37] K. S. Novoselov, V. I. Falko, L. Colombo, P. R. Gellert, M. G. Schwab, K. Kim, *Nature*, **2012**, 490, 192-200.

[38] F. Xia, T. Mueller, Y.-M. Lin, A. Valdes-Garcia, P. Avouris, *Nat. Nanotechnol.,* **2009**, 4, 839-843.

[39] C. L. Tan, Z. D. Liu, W. Huang, H. Zhang, *Chem. Soc. Rev.,* **2015**, 44, 2615-2628.

[40] L. Qu, Y. Liu, J.-B. Baek, L. Dai, *ACS Nano,* **2010**, 4, 1321-1326.

[41] Y. Zheng, Y. Jiao, L. Ge, M. Jaroniec, S. Z. Qiao, *Angew. Chem., Int. Ed.,* **2013**, 52, 3110-3116.

[42] F. Song, X. Hu, *Nat. Commun.,* **2014**, 5, 4477.

[43] J. X. Zhu, D. Yang, Z. Y. Yin, Q. Y. Yan, H. Zhang, *Small*, **2014**, 10, 3480-3498.

[44] Z. Y. Yin, J. X. Zhu, Q. Y. He, X. H. Cao, C. L. Tan, H. Y. Chen, Q. Y. Yan, H. Zhang, *Adv. Energy Mater.,* **2014**, 4, 1300574.

[45] M. F. El-Kady, V. Strong, S. Dubin, R. B. Kaner, *Science*, **2012**, 335, 1326-1330.

[46] Y. F. Sun, S. Gao, Y. Xie, *Chem. Soc. Rev.,* **2014**, 43, 530-546.

[47] X. Peng, L. Peng, C. Wu, Y. Xie, *Chem. Soc. Rev.,* **2014**, 43, 3303-3323.

[48] Z. Liu, J. T. Robinson, X. M. Sun, H. J. Dai, *J. Am. Chem. Soc.,* **2008**, 130, 10876-10877.

[49] K. Yang, L. Feng, X. Shi, Z. Liu, *Chem. Soc. Rev.*, **2013**, 42, 530-547.

[50] Y. Chen, C. L. Tan, H. Zhang, L.Z. Wang, *Chem. Soc. Rev.,* **2015**, 44, 2681-2701.

[51] J. D. Fowler, M. J. Allen, V. C. Tung, Y. Yang, R. B. Kaner, B. H. Weiller, *ACS Nano*, **2009**, 3, 301-306.

[52] F. Yavari, N. Koratkar, *J. Phys. Chem. Lett.,* **2012**, 3, 1746-1753.

[53] C. H. Lu, H. H. Yang, C. L. Zhu, X. Chen, G. N. Chen, *Angew. Chem., Int. Ed.,* **2009**, 48, 4785-4787.

[54] Q. Y. He, S. X. Wu, Z. Y. Yin, H. Zhang, *Chem. Sci.,* **2012**, 3, 1764-1772.

[55] S. X. Wu, Q. Y. He, C. L. Tan, Y. D. Wang, H. Zhang, *Small*, **2013**, 9, 1160-1172.

[56] K. S. Novoselov, A. K. Geim, S. V. Morozov, D. Jiang, Y. Zhang, S. V. Dubonos, I. V. Grigorieva, A. A. Firsov, *Science*, **2004**, 306, 666-669.

[57] J. Wang, F. Ma, M. Sun, *RSC Adv.,* **2017**, 7, 16801-16822.

[58] Y. B. Tang, C. S. Lee, Z. H. Chen, G. D. Yuan, Z. H. Kang, L. B. Luo, H. S. Song, Y. Liu, Z. B. Heand, W. J. Zhang, *Nano Lett.*, **2009**, 9, 1374-1377.

[59] C. Lee, X. Wei, J. W. Kysar, J. Hone, *Science*, **2008**, 321, 385-388.

[60] K. I. Bolotin, K. J. Sikes, Z. Jiang, M. Klima, G. Fudenberg, J. Hone, P. Kim, H. L. Stormer, *Solid State Commun.*, **2008**, 146, 351-355.

[61] B. H. Hong, *Nature*, **2009**, 457, 706-710.

[62] A. A. Balandin, *Nat. Mater.*, **2011**, 10, 569-581.

[63] L. A. Falkovsky, *Phys. Lett. A*, **2008**, 372, 5189-5192.

[64] P. Avouris, Z. Chen, V. Perebeinos, *Nat. Nanotechnol.*, **2007**, 2, 605-615.

[65] A. H. C. Neto, F. Guinea, N. M. R. Peres, K. S. Novoselov, A. K. Geim, *Vacuum*, **2009**, 83, 1248-1252.

[66] A. B. Kuzmenko, H. E. Van, F. Carbone, d. M. D. Van, *Phys. Rev. Lett.,* **2008**, 100, 117401.

[67] J. P. Salvetat, J. M. Bonard, L. Forró, R. Bacsa, T. Stöckli, **1998**, 467-480.

[68] N. Kostoglou, K. Polychronopoulou, C. Rebholz, *Vacuum,* **2015**, 112, 42-45.

[69] J. Eichler, C. Lesniak, *J. Eur. Ceram. Soc.*, **2008**, 28(5), 1105-1109.

[70] C. Janiak, T. M. Klapötke, H.-J. Meyer, “E. Riedel Hrsg.”, *Moderne Anorganische Chemie,* 2. Auflage.

[71] A. Catellani, M. Posternak, A. Baldereschi, AJ. Freeman, *Phys. Rev. B,* **1987**, 36, 6105-11.

[72] N. Ooi, A. Rairkar, L. Lindsley, J. Adams, *J. Phys.: Condens. Matter,* **2006**, 18, 97-115.

[73] S. Yamamura, M. Takata, M. Sakata, *J. Phys. Chem. Solids,* **1997**, 58, 177-183.

[74] Y. Li, J. W. Connell, *Nanoscale,* **2012**, 4, 6908.

[75] O. Hod, *J. Chem. Theory Comput.,* **2012**, 8, 1360-1369.

[76] N. Marom, J. Bernstein, J. Garel, A. Tkatchenko, E. Joselevich, L. Kronik, O. Hod, *Phys. Rev. Lett.,* **2010**, 105, 046801.

[77] K. Watanabe, T. Taniguchi, H. Kanda, *Nat. Mater,* **2004**, 3, 404-409.

[78] K. Watanabe, T. Taniguchi, T. Niiyama, K. Miya, M. Taniguchi, *Nat. Photonics,* **2009**, 3, 591-594.

[79] M. Engler, C. Lesniak, R. Damasch, *Ceram. forum Int.,* **2007**, 84, 49-53.

[80] A. Lipp, K. A. Schwetz, K. Hunold*, J. Eur. Ceram. Soc.*, **1989**, 5, 3-9.

[81] X. Blase, A. De Vita, J.-C. Charlier, R. Car, *Physical Review Letters*, **1998,** 80, 1666.

[82] J.-C. Charlier, X. Blase, A. De Vita, R. Car, *Applied Physics A: Materials Science & Processing*, **1999**, 68, 267-273.

[83] D. Golberg, Y. Bando, *Applied Physics Letters*, **2001**, 79, 415-417.

[84] M. B. Nardelli, C. Brabec, A. Maiti, C. Roland, J. Bernholc, *Physical Review Letters*, **1998**, 80, 313.

[85] A. Pakdel, C. Zhi, Y. Bando, D. Goldberg, *Materials today,* **2012**, 15, 256.

[86] M. Topsakal, E. Aktürk, S. Ciraci, *Phys. Rev. B: Condens. Matter Mater. Phys.*, **2009**, 79, 11544201-11544211.

[87] A. Goriachko, Y. He, A. Marcus Knapp, H. Over, M. Corso, T. Brugger, S. Berner, A. Juerg Osterwalder, T. Greber, *Langmuir*, **2007**, 23, 2928-2931.

[88] A. Bosak, J. Serrano, M. Krisch, K. Watanabe, T. Taniguchi, H. Kanda, *Phys. Rev. B,* **2006**, *73*, 041402.

[89] Q. Peng, W. Ji, S. De, *Comput. Mater. Sci.,* **2012**, *56*, 11.

[90] M. Mirnezhad, R. Ansari, H. Rouhi, *Superlattices Microstruct.,* **2013**, *53*, 223.

[91] T. Han, Y. Luo, C. Wang, *J. Phys. D,* **2014**, *47*, 025303.

[92] I. Jo, M. T. Pettes, J. Kim, K. Watanabe, T. Taniguchi, Z. Yao, L. Shi, *Nano Lett.,* **2013**, *13*, 550.

[93] H. Q. Zhou, J. X. Zhu, Z. Liu, Z. Yan, X. J. Fan, J. Lin, G. Wang, Q. Y. Yan, T. Yu, P. M. Ajayan, J. M. Tour, *Nano Res.,* **2014**, *7*, 1232.

[94] M. T. Alam, M. S. Bresnehan, J. A. Robinson, M. A. Haque, *Appl. Phys. Lett.,* **2014**, *104*, 013113.

[95] L. Liu, S. Ryu, M. R. Tomasik, E. Stolyarova, N. Jung, M. S. Hybertsen, M. L. Steigerwald, L. E. Brus, G. W. Flynn, *Nano Lett.,* **2008**, *8*, 1965.

[96] L. H. Li, Y. Chen, *Adv. Funct. Mater.,* **2016**, 26, 2594-2608.

[97] H. Zhang, *ACS Nano,* **2015**, 9, 9451-9469.

[98] H. Li, G. Lu, Y. Wang, Z. Yin, C. Cong, Q. He, L. Wang, F. Ding, T. Yu, H. Zhang, *Small,* **2013**, 9, 1974-1981.

[99] A. Castellanos-Gomez, L. Vicarelli, E. Prada, J. O. Island, K. L. Narasimha-Acharya, S. I. Blanter, D. J. Groenendijk, M. Buscema, G. A. Steele, J. V. Alvarez, *2D Mater.,* **2014**, 1, 025001.

[100] V. Goyal, D. Teweldebrhan, A. A. Balandin, *Appl. Phys. Lett.,* **2010**, 97, 133117.

[101] L. Liang, K. Li, C. Xiao, S. Fan, J. Liu, W. Zhang, W. Xu, W. Tong, J. Liao, Y. Zhou, *J. Am. Chem. Soc.,* **2015**, 137, 3102-3108.

[102] M. B. Dines, *Mater. Res. Bull*., **1975**, 10, 287-291.

[103] P. Joensen, R. F. Frindt, S. R. Morrison, *Mater. Res. Bull.,* **1986**, 21, 457-461.

[104] J. Zheng, H. Zhang, S. Dong, Y. Liu, C. T. Nai, H. S. Shin, H. Y. Jeong, B. Liu, K. P. Loh, *Nat. Commun.*, **2014**, 5, 2995.

[105] L. H. Li, *J. Mater. Chem.,* **2011**, 21, 11862.

[106] Y. Yao, *Mater. Chem.*, **2012**, 22, 13494.

[107] Y. Lin, T. V. Williams, W. Cao, H. E. Elsayed-Ali, J. W. Connell, *J. Phys. Chem. C,* **2010**, 114, 17434-17439.

[108] J. Y. Huang, H. Yasuda, H. Mori, *J. Am. Ceram. Soc.*, **2004**, 83, 403–409.

[109] A. N. Streletskii, *J. Alloys Compd.*, **2009**, 483, 313-316.

[110] A. Reina, X. Jia, J. Ho, D. Nezich, H. Son, V. Bulovic, M. S. Dresselhaus, J. Kong, *Nano Lett.,* **2009**, 9, 30-35.

[111] X. S. Li, W. Cai, J. An, S. Kim, J. Nah, D. Yang, R. Piner, A. Velamakanni, I. Jung, E. Tutuc, *Science,* **2009**, 324, 1312-1314.

[112] D. Yoo, M. Kim, S. Jeong, J. Han, J. Cheon, *J. Am. Chem. Soc.,* **2014**, 136, 14670-14673.

[113] Z. Q. Sun, T. Liao, Y. Dou, M. S. Hwang, M.-S. Park, , L. Jiang, J. H. Kim, S. X. Dou, *Nat. Commun.*, **2014**, 5, 3813.

[114] R. Amini, S. K. Brar, M. Cledon, R. Y. Surampalli, *J. Hazard. Toxic Radioact. Waste,* **2016**, 20, B4015004-1.

[115] A. Chemelli, F. Goni, L. Fanzott, F. Uhlig, *Small Angle X-ray and Dynamic Light Scattering investigantions of Nanosheets,* **2016**, (Institute of Inorganic Chemistry, Graz University of Technology).

[116] Pecora, *R. Dynamic Light Scattering Applications of Photon Correlation Spectroscopy* (Plenum Press, New York, **1985**).

[117] T. Li, A. J. Senesi, B. Lee, *ACS Chem. Rev.,* **2016**, 116, 11128-11180.

[118] O. Glatter, O. Kratky, "*Small angle X-ray scattering*", **1982**, 102, Academic Press London.

[119] O. Glatter, *J. Appl. Cryst*., **1980**, 13, 577-587.

[120] G. Porod, *Acta. Phys. Austriaca*, **1948**, 2, 255-292.

[121] J. C. Meyer, *Transmission electron microscopy (TEM) of graphene,* **2014**, Woodhead Publishing Limited.

[122] C. T. Koch, *Conventional and Advanced Transmission Electron Microscopy,* **2012**, 36-69, (In-situ Electron Microscopy).

[123] Atkins, *Physical Chemistry*, Sixth edition.

[124] B. Derjaguin, *Acta Phys. Chim.,* **1939**, 10, 333-346.

[125] B. Derjaguin, L. D. Landau, *Acta Phys. Chim.,* **1941**, 14, 633-622.

[126] E. J. W. Verwey, J. T. G., Overbeek, *Theory of Stability of Lyophobic Colloids,* **1948**, Elsevier Amsterdam.

[127] P. Atkins, J. de Paula, *Elements of Physical Chemistry,* Fifth edition.

[128] C. Huang, Ch. Chen, X. Ye, W. Ye, J. Hu, Ch. Xu, X. Qiu, *J. Mater. Chem. A*, **2013**, 1, 12192-12197.

[129] T. K. Mukhopadhyay, A. Datta, *J. Phys. Chem. C,* **2017**, 121, 811-822.

[130] T. J. Mason, J. P. Lorimer*, Applied Sonochemistry: Uses of Power Ultrasound in Chemistry and Processing.*, **2002.**

[131] T. J. Mason, *Sonochemistry, Oxford chemistry Primers,* **1999.**

[132] H. Schnablegger, O. Glatter, *Applied Optics,* **1991,** 30(33), 4889-4896.

[133] S. Guillot, S. Salentinig, A. Chemelli, L. Sagalowicz, M. E. Leser, O. Glatter, *Langmuir,* **2010**, 26(9), 6222-6229.